

# Geochemistry, Geophysics, Geosystems®



## RESEARCH ARTICLE

10.1029/2022GC010772

### Key Points:

- Geological mapping reveals widespread syn-tectonic migmatitic rocks along a main crustal-scale shear zone inside the Lepontine dome
- Alpine nappe emplacement is regionally recorded at 31–33 Ma, locally overprinted in the south by magmatic/fluid pulses at 22–24 Ma
- Mapping and detrital zircon crystals suggest a structurally coherent Cima Lunga unit of pre-Variscan age, as part of the Simano nappe

### Supporting Information:

Supporting Information may be found in the online version of this article.

### Correspondence to:

A. Tagliaferri,  
alessia.tagliaferri@supsi.ch;  
alessia.tagliaferri@unil.ch

### Citation:

Tagliaferri, A., Schenker, F. L., Ulianov, A., Maino, M., & Schmalholz, S. M. (2023). Implications of new geological mapping and U-Pb zircon dating for the Barrovian tectono-metamorphic evolution of the Lepontine dome (Central European Alps). *Geochemistry, Geophysics, Geosystems*, 24, e2022GC010772. <https://doi.org/10.1029/2022GC010772>

Received 9 NOV 2022

Accepted 31 JAN 2023

### Author Contributions:

**Conceptualization:** A. Tagliaferri, F. L. Schenker, S. M. Schmalholz  
**Data curation:** A. Tagliaferri, F. L. Schenker, M. Maino  
**Formal analysis:** A. Tagliaferri  
**Funding acquisition:** F. L. Schenker  
**Investigation:** A. Tagliaferri, F. L. Schenker  
**Methodology:** A. Tagliaferri, F. L. Schenker, A. Ulianov  
**Project Administration:** F. L. Schenker

© 2023 The Authors.

This is an open access article under the terms of the [Creative Commons Attribution-NonCommercial License](#), which permits use, distribution and reproduction in any medium, provided the original work is properly cited and is not used for commercial purposes.

## Implications of New Geological Mapping and U-Pb Zircon Dating for the Barrovian Tectono-Metamorphic Evolution of the Lepontine Dome (Central European Alps)

A. Tagliaferri<sup>1,2</sup> , F. L. Schenker<sup>1</sup> , A. Ulianov<sup>2</sup> , M. Maino<sup>3</sup> , and S. M. Schmalholz<sup>2</sup> 

<sup>1</sup>Institute of Earth Sciences, University of Applied Sciences and Arts of Southern Switzerland (SUPSI), Mendrisio, Switzerland, <sup>2</sup>Institute of Earth Sciences, University of Lausanne (UNIL), Lausanne, Switzerland, <sup>3</sup>Department of Earth and Environmental Sciences, University of Pavia (UNIPV), Pavia, Italy

**Abstract** The Barrovian metamorphism of the Lepontine dome is manifested by isograds that cross-cut tectonic nappe contacts, which is commonly interpreted as metamorphism that occurred after nappe emplacement. However, the pervasive mineral and stretching lineation in amphibolite facies, associated with top-to-foreland shearing, suggests that peak Barrovian conditions are coeval with nappe-overthrusting. Here, we combine mapping and U-Pb zircon dating to better constrain the relation between metamorphism and overthrusting. Metamorphic zircon rims show two age populations at 31–33 and 22–24 Ma. The younger population is locally observed in post-foliation dikes (and associated metasomatism) likely sourced from deep-migmatites exhuming along the Alpine backstop. The older population occurs regionally and is found in syn-kinematic migmatites which occur along a crustal-scale shear zone. Below this shear zone, magmatic and detrital zircon cores suggest that the Cima Lunga unit, previously interpreted as a tectonic mélange with Mesozoic fragments, was a pre-Variscan metasedimentary sequence intruded by Permian granitic sills, now orthogneisses. This unit was strongly sheared along the top of the Simano nappe during overthrusting of a rock pile here-termed Maggia-Adula nappe. This large-scale nappe emplacement imprinted the regional lineation and peak temperatures until 31–33 Ma. Péclet (1–10) and Brinkman (0.002–1.8) numbers, estimated for the overthrusting, suggest an advection-dominated heat transfer caused by rock exhumation, with some diffusion (conduction) during nappe emplacement. Diffusion contributed to Barrovian isograds discordant to the thrust. Shear heating was important if stress times shearing rate  $> \sim 5 \cdot 10^{-6} \text{ W} \cdot \text{m}^{-3}$  within the nappe. The thermal evolution after overthrusting was spatially heterogeneous until ca. 22 Ma.

**Plain Language Summary** The Lepontine area constitutes the core of the Central European Alps. It has a dome structure and it is internally formed by rock units which register pressure and temperature conditions typical of collisional orogens. The temperatures recorded by minerals are high and the origin of the heat that affected the Lepontine units is still unclear. In this study, we implemented different branches of geology to reveal the age of the Alpine events which juxtaposed the Lepontine units, their provenance and evolution. We performed extensive geological mapping to define the lithologies and structures of rocks. From 13 samples, we extracted 1158 zircon crystals that we analyzed and dated. Fieldwork permitted us to discover new rock units and better characterize the transition between the large-scale units constituting the Lepontine dome. We propose a geodynamic scenario involving a major large-scale Alpine unit. The emplacement of this unit generated the main heating event at 31–33 Ma, which is widespread and resulted in peak temperature conditions. The thermal evolution after this event was regionally complex and spatially heterogeneous. Locally in the south we document magmatic/fluid injections at 22–24 Ma, which were sourced from still-hot regions in the roots of the orogen.

## 1. Introduction

Barrovian metamorphism is characterized by a sequence of mineral assemblages associated with increasing metamorphic conditions, from chlorite through biotite, garnet, staurolite, kyanite to sillimanite-bearing (Barrow, 1893, 1912; Jamieson et al., 1998; Tilley, 1925). A Barrovian metamorphic overprint is common in most collisional orogens and in many occurs as concentric metamorphic mineral zones (e.g., Miyashiro, 2012; Winter, 2013). Typical Barrovian temperature ( $T$ ) and pressure ( $P$ ) conditions correspond to ca. 450–750°C and ca. 0.5 up to 1 GPa (ca. 20–40 km lithostatic depth), respectively (e.g., Jamieson et al., 1998). However,

**Resources:** F. L. Schenker

**Supervision:** F. L. Schenker, S. M. Schmalholz

**Validation:** A. Tagliaferri, F. L.

Schenker, A. Ulianov, M. Maino, S. M. Schmalholz

**Visualization:** A. Tagliaferri, F. L. Schenker

**Writing – original draft:** A. Tagliaferri, F. L. Schenker, S. M. Schmalholz

**Writing – review & editing:** A. Tagliaferri, F. L. Schenker, A. Ulianov, M. Maino, S. M. Schmalholz

the geodynamic interpretation of such temperatures, which are higher than typical subduction zone geotherm conditions, remains debated. The main reason for this debate is that the relative importance of the controlling heat sources, such as radiogenic heat production or shear heating, and of the associated heat transfer processes, such as heat diffusion (in this work equivalent to heat conduction) and heat advection by kilometer-scale exhuming rock units, as well as the heat transport associated with fluid and melt migration, is still unclear (e.g., Burg & Gerya, 2005; Jamieson et al., 1998; Thompson & Ridley, 1987).

In the Lepontine dome of the Central Alps, Barrovian metamorphism is associated with a dome structure that comprises a pile of tectonic nappes, including the Adula, Maggia and Simano nappes (Figure 1), which are separated by major shear zones (e.g., Berger et al., 2005; Frey & Ferreiro Mählmann, 1999; Nagel, 2008; Rosenberg et al., 2021; Todd & Engi, 1997; Trommsdorff, 1974; Wenk & Keller, 1969; Figure 1). In the Lepontine area, the metamorphic isograds cross-cut the tectonic nappe boundaries (e.g., Frey & Ferreiro Mählmann, 1999; Nagel, 2008; Todd & Engi, 1997; Trommsdorff, 1974; Wenk & Keller, 1969; Figure 1). This observation is frequently interpreted as evidence for a Barrovian overprint that occurred after nappe emplacement, defining the Barrovian metamorphism as post-nappe or post-tectonic (e.g., Frey et al., 1999; Nagel, 2008; Todd & Engi, 1997; Trommsdorff, 1974; Wenk & Keller, 1969). However, Barrovian metamorphism had already begun by ca. 32 Ma (e.g., SHRIMP II U-Pb zircon dating in Galli et al. (2012); SHRIMP U-Pb dating in Gebauer (1996)), which corresponds to the late stage of nappe emplacement, that is between 31 and 33 Ma for the Adula nappe (e.g., Herwartz et al., 2011; SHRIMP U-Pb zircon dating in Liati et al., 2009; Nagel, 2008). In principle, it is possible that nappe emplacement contributed significantly to the heat transfer responsible for the regional Barrovian metamorphism. Heat is indeed advected and produced during nappe exhumation and overthrusting. Furthermore, heat can be transferred by diffusion to the colder units adjacent to the overthrusting nappe (e.g., England & Molnar, 1993; Huerta et al., 1998; Oxburgh & Turcotte, 1974; Thigpen et al., 2017), hence, it can generate metamorphic isograds that cross-cut nappe boundaries (e.g., Huerta et al., 1998; Thigpen et al., 2017, 2021). Therefore, the evidence of cross-cutting relationships between isograds and tectonic boundaries does not exclude a syn-tectonic origin of the Barrovian metamorphism.

In addition to the timing, the tectonic processes responsible for the Barrovian metamorphism are also debated. Several interpretations and models have been proposed, such as (a) post-tectonic (after nappe emplacement) thermal relaxation through far-field conductive heating (e.g., Bousquet et al., 1997), (b) post-tectonic heating related to deeper processes such as slab breakoff, slab retreat, or lower crust delamination (e.g., Brouwer et al., 2004; Herwegh et al., 2017; Schlunegger & Kissling, 2015), (c) tectonic juxtaposition of slices of highly radiogenic crust and associated radiogenic heating (e.g., Engi et al., 2001), (d) syn-tectonic in situ heat production by shear heating during orogenic wedge formation (e.g., Burg & Gerya, 2005), or (e) superposition of different processes at different stages, such as accretion of hot middle crust material within a subduction channel and underplating of hot material during continental lower plate accretion (e.g., Berger et al., 2011). In order to test such models and unravel the tectono-metamorphic processes responsible for the Barrovian metamorphism, detailed geological maps and cross sections, structural analysis as well as geochronological data are necessary. Without an improved knowledge of the current nappe geometries and kinematic evolution of the Lepontine nappes, the interpretation of the Barrovian metamorphism remains difficult. This is true also for the rest of the Alps, which have been studied for more than a century, but they are still arguably one of the most controversially interpreted orogens. For example, in the Lepontine area both the paleogeographic origin and the current structural position of the Maggia nappe within the Lepontine nappe pile are debated (e.g., Maxelon & Mancktelow, 2005; Schmid et al., 2004; Steck et al., 2019; see also next Section 2.2.3). In addition, the Cima Lunga has recently been the center of a renewed debate concerning the origin of its high-pressure rocks, either formed during the deep burial history of the unit or at shallower depths with pressures deviating from lithostatic conditions (crf., Corvò et al., 2021; Maino et al., 2021; Piccoli et al., 2021). Therefore, we present here the results of a tectono-metamorphic study comprising (a) detailed geological mapping and structural analysis (macro-, meso-, and micro-scale) built on the new large-scale geological maps of *Osogna n°1293*, *Biasca n°1273*, *Grono n°1294* of the Swiss National Map 1:25,000 (mapping at scale 1:10'000), which we produced at the University of Applied Sciences and Arts of Southern Switzerland (SUPSI) for swisstopo, (b) collection and description of representative samples (e.g., syn-tectonic migmatites) in specific localities (at tectonic contacts and inside the nappes) and (c) Laser Ablation Inductively-Coupled Plasma Mass Spectrometry (LA-ICP-MS) and Secondary Ion Mass Spectrometry (Swiss-SIMS) U-Pb geochronology and geochemistry (LA-ICP-MS trace element analyses) on zircon crystals. Specific aims of our study are (a) to pinpoint the age of the peak *T* metamorphism characterizing the Lepontine area with

U-Pb zircon dating, by investigating the ages of syn-kinematic migmatites observed along major tectonic nappe boundaries, (b) to investigate the structural style (coherent vs. tectonic mélange) and age of the Cima Lunga unit as well as its structural relation with the Simano and Adula nappes, (c) to discuss the paleogeographic and tectonic relationship between the major tectonic nappes in the Lepontine dome, namely the Simano nappe, the Cima Lunga unit and the Maggia and Adula nappes and hence (d) to propose a revised geodynamic interpretation for peak Barrovian metamorphism in the Lepontine dome.

We start with a geological overview of the Lepontine dome, followed by a description of sampling and dating methodology. Afterward, due to the large amount of new data from several localities, we present together the results and interpretation of data from mapping, sample description, and dating for each locality. Finally, we integrate information from all the studied areas, providing a general discussion about the timing and mechanisms of the Barrovian metamorphism in the Lepontine dome.

## 2. Geological Overview

### 2.1. Tectonic Overview and Formation of the Lepontine Dome

The Central Alps formed as a consequence of the closure of the Mesozoic Ligure-Piemontese basin(s) (e.g., Handy et al., 2010; Stampfli et al., 1998; Trümpy, 1973). This closure involved the south-verging subduction of the Ligure-Piemontese unit and the European passive margin under the Adriatic (African) plate, which started in the middle Cretaceous (e.g., Handy et al., 2010; Rosenbaum & Lister, 2005; Stampfli et al., 1998; Trümpy, 1973; Zanchetta et al., 2012). In the more proximal domains of the extended paleo-European passive margin, nappe stacking started in the vanishing stage of oceanic subduction and continued during continental collision (e.g., Coward & Dietrich, 1989; Hurford, 1986; Schmid et al., 1996). In the Penninic domain of the Central Alps, the transition from oceanic subduction to continent-continent collision occurred between the Eocene and Early Oligocene (e.g., Gebauer, 1996; Schmid et al., 1990, 1996; Wiederkehr et al., 2009). In the frontal Penninic domain,  $^{40}\text{Ar}/^{39}\text{Ar}$  dating of biotite and white mica constrains the Eocene sediment accretion and subduction at 40–42 Ma, and the nappe stacking at 33–36 Ma (Wiederkehr et al., 2008, 2009). The basement nappes were stacked from south to north forming a crustal nappe stack, which was later up-arched to form the Lepontine dome (Merle et al., 1989; Steck & Hunziker, 1994; Steck et al., 2013). Its architecture is subdivided in two sub-domes: the so-called Toce culmination to the west and the Ticino culmination to the east (Figure 1a). The Ticino culmination, subject of this study, exposes in its core the Leventina and Simano nappes that are flanked to the east by the Adula nappe and to the west by the Cima Lunga unit and the Maggia nappe (Figure 1; e.g., Dal Vesco, 1953; Maxelon & Mancktelow, 2005; Steck et al., 2013).

### 2.2. The Lepontine Nappes

#### 2.2.1. The Simano Nappe

The lower tectonic units in our study area are the Leventina and Simano nappes (Figures 1b and 1c). The Simano nappe is a metamorphosed intrusive complex formed by several Ordovician and Carboniferous magmatic bodies (Köppel et al., 1981), the latter intruding pre-Mesozoic paragneisses (Jenny, 1923; Wenk & Keller, 1969). To the north, the Simano nappe was thrust over the Leventina nappe, forming a fold nappe. Based on multiple-equilibrium thermobarometry, Alpine metamorphism peaked at ca. 0.6 GPa and 625°C without preserved evidence of an Alpine eclogitic precursor (e.g., Allaz et al., 2005; Rütli, 2001; Rütli et al., 2005, 2008).

#### 2.2.2. The Cima Lunga Unit

To the west, the Simano nappe is overlaid by the Cima Lunga unit that comprises paragneisses, orthogneisses, sheets of marble and calcschist, as well as mafic and ultramafic rocks (Figures 1b and 1c). The latter outcrop as lenses or boudinaged layers due to the intense deformation (e.g., Becker, 1993; Corvò et al., 2021; Evans et al., 1979; Maino et al., 2021; Pfeifer, 1981). The Cima Lunga unit differs lithologically from the other Penninic nappes (Leventina, Simano and Maggia) in the more frequent occurrence of ultramafic bodies and eclogites. Eclogitic metarodigites within ultramafic lenses testify metasomatism and serpentization prior to the Alpine eclogitic metamorphism and deformation (Evans & Trommsdorff, 1978; Evans et al., 1979; Pfiffner & Trommsdorff, 1997, 1998). Eclogitic conditions occurred at ca. 40 Ma (Becker, 1993) before decompression until ca. 32 Ma (Becker, 1993; Berger et al., 2011; Brouwer & Engi, 2005; Corvò et al., 2021; Gebauer, 1994, 1996, 1999). The peak pressure

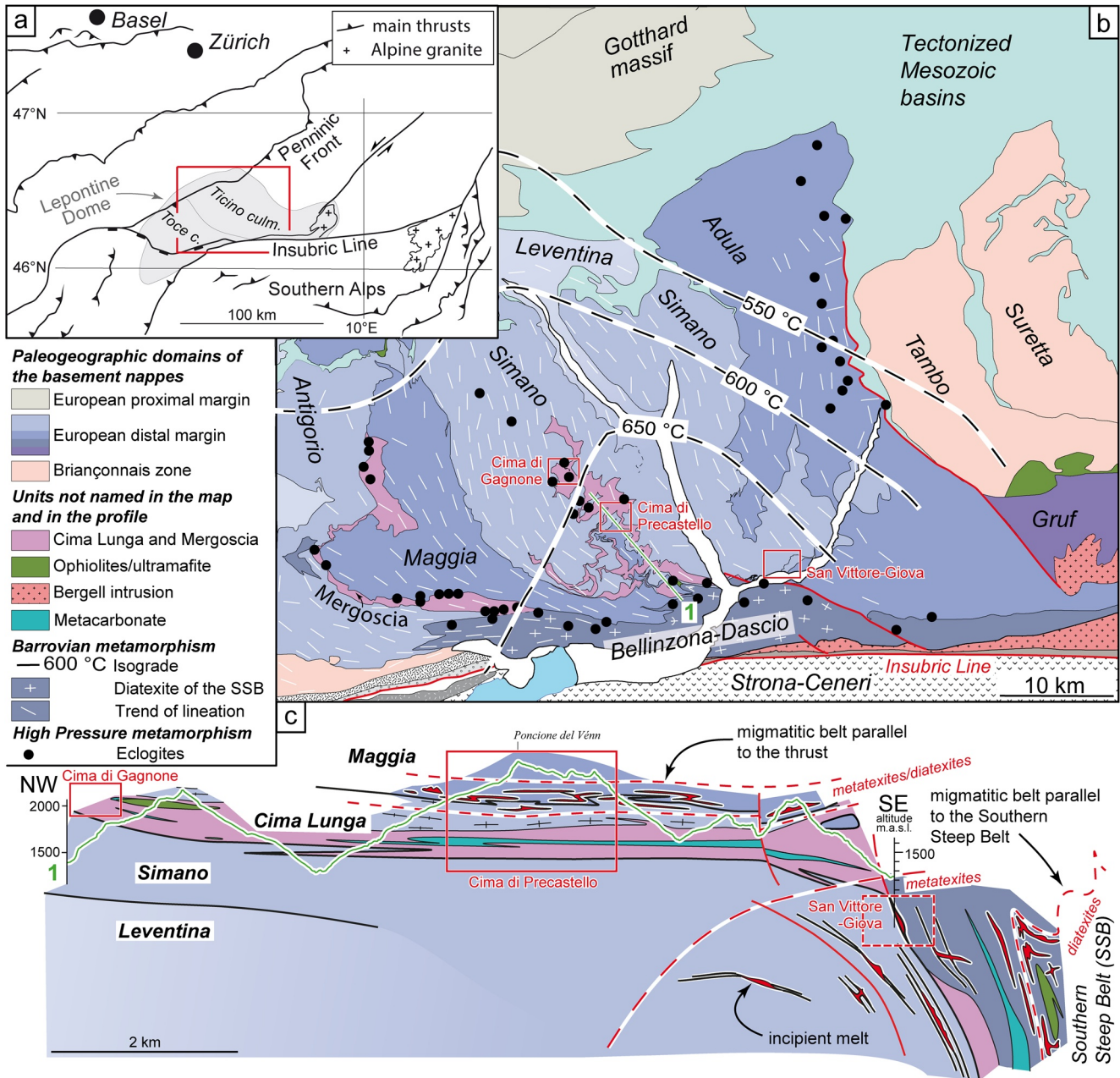


**Figure 1.** Tectonic overview of the Lepontine area. (a) Location of the Lepontine dome in the Central European Alps context (modified after Burg and Gerya (2005)). (b) Tectonic map of the Ticino culmination of the Lepontine dome (modified after Brouwer et al. (2005); Cavargna-Sani, Epard, & Steck, 2014; Corvò et al., 2021; Maino et al., 2021; Steck et al., 2013; Todd & Engi, 1997; Wenk, 1955). (c) Simplified tectonic profile (Profile 1) through the central domain of the Ticino culmination. The red boxes indicate the studied areas (Cima di Gagnone, Cima di Precastello, San Vittore-Giova).

condition reached 2.0–3.0 GPa at 650–850°C in the ultramafic lenses (Evans et al., 1979; Heinrich, 1982; Nimis & Trommsdorff, 2001; Pfiffner, 1999; Scambelluri et al., 2014) and 1.5–2.5 GPa at 600–700°C in the eclogites (Heinrich, 1986). It was even proposed that peak pressures may have reached extreme conditions of at least ca. 5.9 GPa at ca. 1180°C in the garnet peridotite lens at Alpe Arami (e.g., Dobrzhinetskaya et al., 1996; Paquin & Altherr, 2001). However, these extreme conditions are disputed (e.g., Nimis & Trommsdorff, 2001).

The bulk of the Cima Lunga unit is made of paragneisses characterized by dominant amphibolite-facies conditions (peak  $P$  of 0.6–0.8 GPa and peak  $T$  of 600–675°C) with local evidence of high-pressure (HP) and high-temperature (HT) mineral assemblages (up to 2.7 GPa and 850°C; Corvò et al., 2021; Grond et al., 1995;

Heinrich, 1982; Piccoli et al., 2021; Pfiffner, 1999). HP-HT conditions are attributed to either extreme depth reached by the whole unit during subduction (Piccoli et al., 2021) or local coexisting heterogeneous metamorphic equilibria driven by deformation (Corvò et al., 2021).

The Cima Lunga unit is commonly interpreted to connect to the east with the Adula nappe (e.g., Dal Vesco, 1953; Trommsdorff et al., 2000). To the west, Steck et al. (2013) proposed its tectonic correlation with the Mergoscia zone, which is an eclogitic HP unit at the top of the Antigorio nappe and enveloping the bottom of the Maggia nappe. To the south, the Cima Lunga unit is tectonically overlaid by the Maggia nappe (Steck et al., 2013).

### 2.2.3. The Maggia Nappe

The Maggia nappe is dominated by orthogneisses with (mostly) Permian intrusion ages (Bussien et al., 2011; Köppel et al., 1981; Steiner, 1984), which are enveloped by polymetamorphic sedimentary rocks (Günther et al., 1996). Some of these meta-sedimentary rocks show pre-Silurian sedimentation ages (Köppel et al., 1981). Amphibolitic zones are also present, and ultramafic lenses are sparsely scattered (e.g., Buchmann, 1953; Della Torre et al., 2015; Preiswerk, 1918). The frontal part of the Maggia nappe is in contact with the Simano and the Antigorio gneisses and the Mesozoic sedimentary cover. There, the structures remain controversial due to the complex superposed folding along the “Maggia-querzone” that locally reverses the tectonostratigraphy along the NW–SE directed fold axes. Accordingly, different interpretations have been suggested for the paleogeographic origin of the Maggia nappe. The Maggia nappe has been attributed to (from the distal to the proximal domains): (a) the Briançonnais domain (Froitzheim et al., 1996; Schmid et al., 2004), (b) the Lower Penninic domain (Grujic & Mancktelow, 1996; Steck, 1998; Steck et al., 2013), (c) the Helvetic domain (Debelmas & Lemoine, 1970; Rütli et al., 2005; Steck et al., 2019), or (d) both the Briançonnais (the southern part) and Helvetic (the northern part) domains (Sambuco lobe, Berger et al., 2005).

### 2.2.4. The Adula Nappe

On the eastern flanks of the dome, the Simano nappe was overthrust by the Adula nappe, which is dominated by orthogneisses and paragneisses, quartzite sheets, calcitic and dolomitic marbles, calcschists, and lenses of eclogitic mafic and ultramafic rocks (Cavagna-Sani, Eppard, Bussy, & Ulianov, 2014; Jenny, 1923; Nagel, 2008). Here, peak *P* metamorphism (eclogitic) is restricted to mafics, ultramafics and whiteschist lenses, and to minor volumes of paragneisses (Brouwer & Engi, 2005; Heinrich, 1982; Meyre et al., 1998) reaching up to ca. 3 GPa at 800°C (Dale & Holland, 2003; Nimis & Trommsdorff, 2001; Tumiatì et al., 2018). The activity of the Adula thrust is bracketed between the eclogitization at 38–40 Ma and the peak of Barrovian metamorphism at ca. 32–33 Ma (Herwartz et al., 2011; Liati et al., 2009; Nagel, 2008; Sandmann et al., 2014). The Adula nappe and the Cima Lunga unit are generally interpreted in the literature as parts of the same tectonic nappe (e.g., Dal Vesco, 1953).

## 2.3. The Barrovian Metamorphism

The Lepontine dome exposes IP (Intermediate Pressure)-HT (High Temperature) rocks, indicative of Barrovian metamorphic conditions, ranging from migmatites to lower amphibolite-greenschist facies. Minor volumes of (ultra-)HP rocks are also present within the rocks of the Barrovian sequence. The overall metamorphic trend of the Lepontine dome shows high-grade (upper amphibolite facies) migmatites at the southern margin, along the Southern Steep Belt (SSB), and lower amphibolite-greenschist facies rocks in the dome carapace (Figure 1, northern and eastern parts). Peak *T* increases from 500 to 550°C at the northern margin of the dome, defined by the Northern Steep Belt (NSB; Frey, 1969; Janots et al., 2008), to ca. 700 ± 50°C at its southern margin along the SSB (Burri et al., 2005). The mineral-zone boundaries and the isograds of this Tertiary metamorphism show an asymmetric zonation. This zonation does not coincide with the dome shape, which is defined by the regional attitudes of foliation and thrust sheets (e.g., Maxelon & Mancktelow, 2005; Merle et al., 1989; Todd & Engi, 1997; Wenk, 1955; Wenk & Keller, 1969). In fact, the Barrovian isograds depict concentric shells locally dissecting the tectonic nappe contacts (Figure 1). Most P-T paths for the Lepontine nappes show a single clockwise path with the amphibolitic climax reached at close to peak *P* or during decompression from HP (e.g., Brouwer et al., 2004; Nagel, 2008; Rütli et al., 2008). The final isothermal decompression of the (U)HP units (Adula nappe and Cima Lunga unit, e.g., Brouwer et al., 2004; Nagel, 2008) at amphibolitic condition of 650–700°C at ca. 0.8 GPa occurred at or before 32 Ma (zircon U-Pb SHRIMP; Galli et al., 2012; Gebauer, 1996). Some rocks in the SSB and NSB record instead a two-stage thermal event articulated in an isobaric heating to peak *T* after decompression from HP (e.g., Bousquet et al., 2008; Wiederkehr et al., 2008). The peak *T* metamorphism in the SSB lasted from 32 to 22 Ma within a long-lasting episodic migmatitic event, as constrained by different geochronometers (allanite

U-Th-Pb SHRIMP in Gregory et al. (2012); zircon U-Pb SHRIMP in Rubatto et al. (2009)). In the NSB, prograde syn-tectonic garnets nucleated and grew during the Alpine metamorphism and were dated at 25.4 Ma (Lu-Hf garnet-rutile; Berg et al., 2013). Along the NSB, peak *T* metamorphism started later between 25 and 19 Ma at lower temperatures than the southern units (Berg et al., 2013; Janots et al., 2009; Wiederkehr et al., 2011).

Across the Lepontine dome, Boston et al. (2017) reported allanite U-Th-Pb age data, providing evidence that nappe stacking at prograde amphibolite facies conditions and refolding occurred between 32 and 27 Ma. Younger U-Th-Pb monazite ages (until ca. 19 Ma) are interpreted as post-collisional mineral growth close to peak *T* (Boston et al., 2017). After ca. 19 Ma, the Lepontine dome cooled from 500°C to 120°C (zircon fission track) relatively homogeneously until ca. 6 Ma as shown by low-*T* geochronometers (Hurford, 1986; Janots et al., 2009). Within this diachronous metamorphic history, the discordant metamorphic isograds are considered to form during late conductive heating at ca. 19 Ma (e.g., Berger et al., 2011).

## 2.4. Structures

Regionally, all lithologies show a sub-horizontal penetrative foliation, formed at peak *T* condition (Figure 2). This foliation dips gently along the dome flanks forming a bell-shaped architecture. The foliation intensity varies with rock-type (see Figure 2) and structural position. The alternation of lithotypes is mostly parallel to the nappe boundaries, and constant over its kilometer-scale length (Swiss National Map no. 1293 - Osogna (1:25,000)). Intra-foliation folds with axial planes sub-parallel to the foliation and fold axes oriented close to NW-SE trend are common. Furthermore, sheath folds are common in some units (e.g., in gneissic rocks enveloping ultramafics of the Cima Lunga unit; Maino et al., 2021; Steck et al., 2019) and show complex deformation patterns in the field.

On the foliation, an extremely pervasive NW-SE directed mineral and stretching lineation points to non-coaxial deformation at peak Barrovian metamorphic conditions. The orientation of the lineation is independent of the foliation attitude. Independently of the position within the concentric dome isograds, the ubiquitous linear fabric is defined by minerals of the peak *T* assemblage, such as biotite flakes, amphiboles and kyanite, as well as stretched lithons (Maino et al., 2021; Swiss National Map no. 1293 - Osogna (1:25,000); Wenk & Keller, 1969). The penetrative character of the linear fabric within the dome core (see Figure 1) suggests that the constrictional (axes of the strain ellipsoid:  $X > Y = Z$ ) deformation event likely occurred during shearing coeval with nappe emplacement and regional amphibolite facies metamorphism. However, the absolute timing of the upper-amphibolitic, non-coaxial deformation along the tectonic contacts is still poorly constrained.

### 2.4.1. Migmatites

Alpine migmatites have been observed in the SSB trending E-W parallel to the Insubric Line (Figure 1, Burri et al., 2005; Gebauer, 1994, 1996; Rubatto et al., 2009), and within the Cima Lunga paragneisses (Corvò et al., 2021; Pfiffner, 1999). Wenk and Keller (1969) also mapped migmatites further north of the SSB, although these are generally interpreted as pre-Alpine (e.g., Burri et al., 2005). Burri et al. (2005) suggested that some of these migmatites (15 km north of the SSB, Maggia Valley) could have an Alpine age, however there is no chronometric data confirming this hypothesis. In the migmatites of the SSB, U-Pb ages on metamorphic zircon rims and allanite bracket the peak *T* conditions after the HP event between 32 Ma and 22 Ma (Gebauer, 1999; Gregory et al., 2012; Rubatto et al., 2009). These ages and the relative distribution of zircon overgrowths were interpreted as repeated melting events within a single Barrovian metamorphic cycle. This melting was due to a combination of water-assisted and muscovite-dehydration partial melting, which occurred at roughly constant *T* and minimal *P* variations ( $700 \pm 50^\circ\text{C}$  and 0.6–0.8 GPa; Berger et al., 2008; Burri et al., 2005; Rubatto et al., 2009).

The Cima Lunga migmatites around an ultramafic HP lens dated by Corvò et al. (2021) at ca. 36 Ma were instead considered as melts formed during decompression from 2.5 to 1.5 GPa at ca. 750–850°C.

Most syn-tectonic migmatites reported in this study (Figure 2) were not previously reported in the literature or were considered as pre-Alpine. The overall timing of this partial melting is important to correlate the close-to-peak *T* conditions that the migmatites are thought to have formed at, with deformation along the nappe boundaries.

## 3. Sampling and Dating Methodology

### 3.1. Sample Collection and Preparation

We performed detailed geological mapping coupled with structural analysis in three key areas of the central-southern Lepontine dome to study the upper-amphibolitic deformation at different tectonostratigraphic levels of the nappe

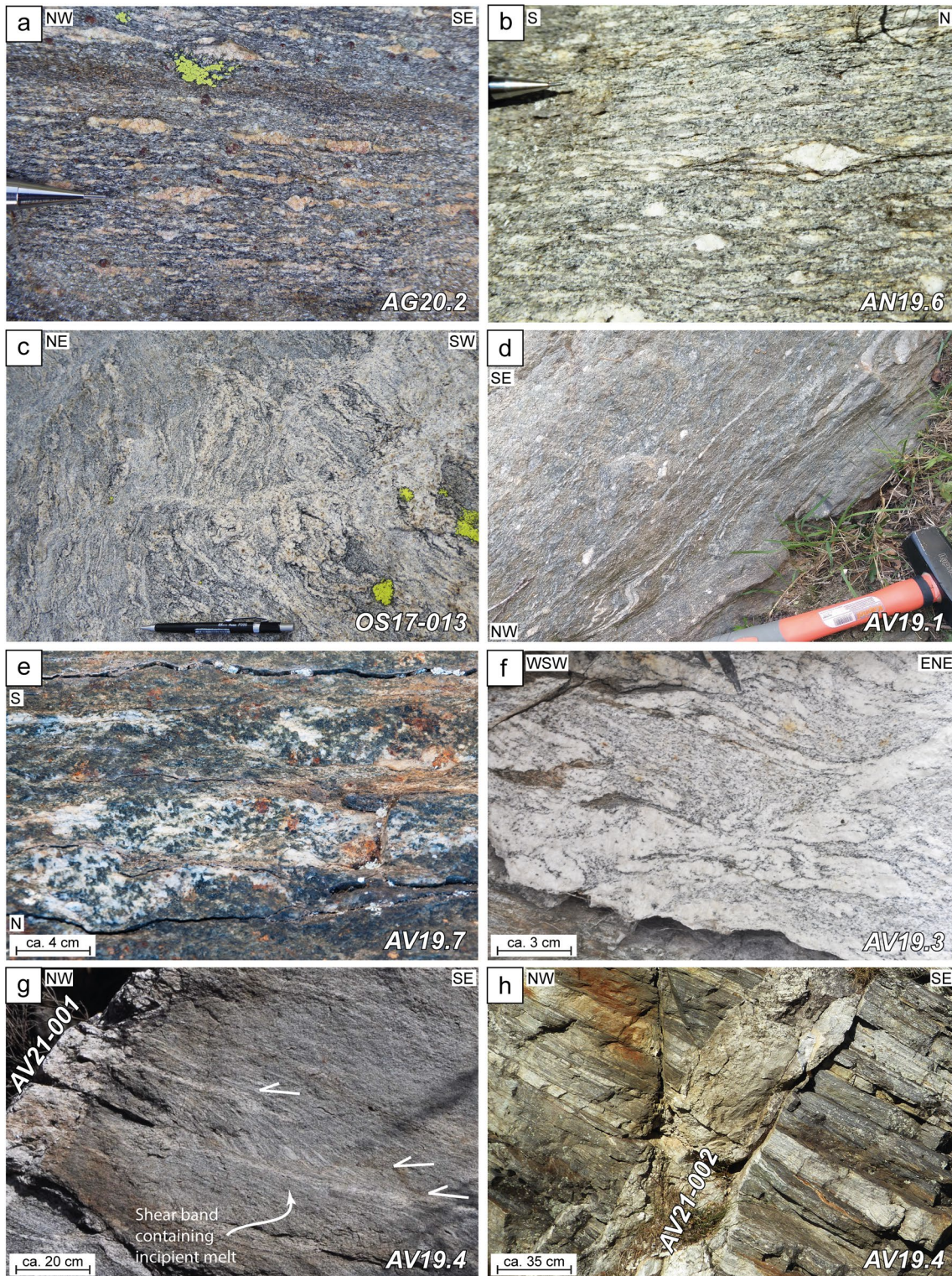


**Figure 2.** Field occurrence of the analyzed lithotypes. (a) Leucocratic pods in the (partially) migmatitic garnet-paragneiss AG20.2 in Cima di Gagnone (Cima Lunga unit). (b) Feldspar augen in the foliation of the leucocratic orthogneiss AN19.6 in Cima di Precastello (Cima Lunga unit). (c) Diffuse leucosomes in OS17-013 migmatitic orthogneiss in Cima di Precastello (base of Maggia nappe). (d) Sheared quartz veins in the AV19.1 metaconglomerate in San Vittore (Simano-Adula nappe contact). (e) Detail of the migmatitic garnet-paragneiss AV19.7 in San Vittore (Simano-Adula nappe contact). (f) Detail of a deformed leucosome network in the syn-tectonic migmatites AV19.3 in San Vittore (Simano-Adula nappe contact). (g) Syn-tectonic migmatites AV19.4 in Giova (base of Simano nappe) with leucosomes within shear bands. The migmatitic foliation is sharply cut by the AV21-001 pegmatitic dike. (h) The m-scale aplitic to pegmatitic dike AV21-002 cuts the migmatitic and mylonitic foliation of AV19.4 in Giova.

**Table 1**  
*Samples, Locations, and Zircon Characteristics*

Tectonic nappe	Study area	Sample Rock type	Mineral assemblage*	Zircon main textural features	Interpreted zircon origin and Th/U ratio			Swiss grid coordinates (CH1903+/LV95)	
					Origin	Th/U ratio: range median (n)	Age (Ma) (2σ error)	E	N
Cima Lunga	Cima di Gagnone	AG19.5 <i>Quartzofeldspathic gneiss</i>	qtz, feld, bt, wm, chl, st, zr, ep	125-250 μm Anhedral to subhedral Uneven edges Micro-cracks	DR	0.097 (1)		2708973	1132336
						0.128-0.291 (5)			
						0.345-1.87 (11)			
		AG19.6 <i>Grt-paragneiss</i>	qtz, feld, grt, bt, wm, chl, ky, st, zr, ep, rt, ap, ox	200 μm Anhedral	DR	0.003-0.814 0.339 (14)	276.76 ± 3.56	2708804	1132391
						0.0015-0.040 0.002 (7)	39.42 ± 1.29 31.47 ± 0.50		
		AG20.1 <i>Migmatitic grt-paragneiss</i>	qtz, feld, grt, bt, wm, chl, zr, ep, rt, ttn, ox	60-150 μm Anhedral to subhedral	DR	0.189 (1)	282.87 ± 5.50	2708891	1135441
						0.414-0.613 (2)			
		AG20.2 <i>Migmatitic grt-paragneiss</i>	qtz, feld, grt, bt, chl, zr, rt, cld, ox	125-250 μm Anhedral to subhedral Uneven edges	DR	0.448-1.110 0.840 (3) [CORE]	548.76 ± 10.57	2708333	1131210
						0.016-0.052 0.031 (5) [RIM]			
		AG20.2 <i>Migmatitic grt-paragneiss</i>	qtz, feld, grt, bt, chl, zr, rt, cld, ox	125-250 μm Anhedral to subhedral Uneven edges	DR	0.002 (1)	315.30 ± 16.71	2708337	1131193
	0.161-0.231(2) 0.507-1.330 (3)								
	AG20.2 <i>Migmatitic grt-paragneiss</i>	qtz, feld, grt, bt, chl, zr, rt, cld, ox	125-250 μm Anhedral to subhedral Uneven edges	DR	0.094-0.974 0.620 (3)	687.09 ± 23.82	2708333	1131210	
					0.005-0.007 0.006 (5)	31.42 ± 0.65			
	AG20.2 <i>Migmatitic grt-paragneiss</i>	qtz, feld, grt, bt, chl, zr, rt, cld, ox	125-250 μm Anhedral to subhedral Uneven edges	DR	0.219-0.284 (2)	315.30 ± 16.71	2708337	1131193	
					0.378-0.870 (14)				
AG20.2 <i>Migmatitic grt-paragneiss</i>	qtz, feld, grt, bt, chl, zr, rt, cld, ox	125-250 μm Anhedral to subhedral Uneven edges	DR	0.002-0.003 (2)	30.99 ± 0.42	2708337	1131193		
				0.001-0.010 0.004 (41)					
Cima di Precastello	AN19.6 <i>Quartzofeldspathic gneiss</i>	qtz, feld, bt, chl, wm, zr, rt, ox	100-250 μm Anhedral to subhedral Uneven edges	MG	0.154-0.717 0.278 (28)	277.74 ± 2.82	2713614	1127870	
Maggia	Cima di Precastello	OS17-013 <i>Migmatitic orthogneiss</i>	qtz, feld, bt, wm, chl, zr, ap	100-250 μm Anhedral to subhedral Uneven edges	MG	0.056-0.334 0.147 (13)	281.01 ± 2.86	2712677	1126237
						0.0006-0.009 0.002 (40)	31.36 ± 0.27		
Simano-Adula	San Vittore-Giova	AV19.1 <i>(Migmatitic) Meta-conglomerate</i>	qtz, feld, bt, wm, chl, zr, ep, ap, ox	90-250 μm Idiomorphic to anhedral	DR	0.002-0.080 (13)	31.15 ± 0.32	2728908	1122413
						0.164-0.269 (12)			
						0.322-1.735 (54)			
		AV19.7 <i>Migmatitic grt-paragneiss</i>	qtz, feld, grt, bt, wm, chl, ky, st, zr, ep, rt, ap, amph, cld, ox	200 μm Anhedral, some idiomorphic	DR	0.001-0.015 0.004 (26)	34.75 ± 0.83 31.53 ± 0.68	2728838	1122423
						0.048-0.064 (2)			
						0.200-0.278 (8) 0.309-1.210 (17)			
	AV19.3 <i>Migmatitic orthogneiss</i>	feld, qtz, bt, wm, chl, zirc, ep, ox, amph	125-250 μm Subhedral to anhedral Uneven edges	MG	0.002-0.009 0.005 (7)	282.07 ± 1.79	2728407	1122398	
					0.154-0.982 0.406 (37)				
					0.0005-0.016 0.0039 (13)				30.99 ± 0.41
	AV19.4 <i>Migmatitic orthogneiss</i>	feld, qtz, bt, wm, chl, zirc, ep, ap, ox	125-250 μm Subhedral to anhedral Uneven edges	MG	0.001-0.114 0.006 (16)	278.41 ± 4.99	2728425	1123530	
					0.013-0.661 0.450 (8)				22.46 ± 0.69
	AV21-001 <i>Pegmatitic dike</i>	feld, wm, qtz, grt, zirc	100-150 μm Sub-idiomorphic Uneven edges	MG	0.002-0.016 0.006 (9)	23.00 ± 0.14	2728422	1123526	
0.003-0.013 0.006 (20)									
AV21-002 <i>Granitic dike</i>	feld, qtz, wm, bt, chl, zirc, rt, ep, ox	50-100 μm Anhedral to subidiomorphic	MG	0.003-0.004 0.004 (6)	22.57 ± 0.31	2728187	1123488		
				0.064-0.066 (2)				21.56 ± 0.62	

*Note.* Mineral abbreviations\* are reported in Supporting Information S1 (*THINSECTIONS\_description.docx*). Zircon origin is indicated as: DR = detrital, MG = magmatic, ME<sub>V</sub> = metamorphic (Variscan), ME<sub>A</sub> = metamorphic (Alpine). Th/U ratios are reported with their range and median value, *n* = number of analyses. Detrital zircon crystals are subdivided according to Teipel et al. (2004). Th/U is calculated from LA-ICP-MS data (see Supporting Information S1 *UPb\_LAICPMS folder*) and ages are LA-ICP-MS Concordia ages with 2σ error (only one SIMS Pb<sup>206</sup>/U<sup>238</sup> age with its relevant Th/U is reported in italics: single data from *UPb\_SIMS.xlsx*). The distribution of dates for detrital zircon grains is in Supporting Information S1 *KDE\_LAICPMS.pdf*.

pile and at different horizontal distances with respect to the migmatites of the SSB (Figure 1): (a) the Cima di Gagnone area of the Cima Lunga unit, located in the center of the dome and at a distance of ca. 15 km from the SSB (Figure 3), (b) the Cima di Precastello area at the Cima Lunga-Simano-Maggia nappe boundary, at ca. 8 km distance from the SSB (Figure 4), and (c) the San Vittore-Giova area located at the Simano-Adula nappe contact at the northern margin of the SSB (Figure 5). The geological maps relevant to these three areas are the result of our own original geological mapping at the scale 1:10'000 and structural data measured in the field. The map of the Cima di Gagnone area was already published by Maino et al. (2021) and Corvò et al. (2021). Overall, 13 samples were collected at different tectonic levels for U-Pb zircon dating (Table 1).

Zircon grains were separated at the University of Lausanne by standard grinding followed by sieving (125–250  $\mu\text{m}$  fraction was selected), panning, magnetic separation and heavy liquid procedures. For some samples (*Sample OS17-013; AV21-001; AV21-002; AN20.1; AG20.1; AG20.2*), a Wilfley table at ETH Zurich was used for zircon extraction. Zircon grains were subsequently cast in epoxy resin to form mounts which were polished down to expose grain centers.

### 3.2. Analytical Techniques

Cathodoluminescence (CL) imaging was carried out at the Scanning Electron Microscope laboratory of the University of Lausanne using a CamScan MV2300 electron microscope. CL-images were used to set point analyses on the target zircon domains.

Analyses were performed using LA-ICP-MS (Laser Ablation Inductively-Coupled Plasma Mass Spectrometry) and SwissSIMS ion probe (Secondary Ion Mass Spectrometry) facilities at the University of Lausanne. Laser spot diameter for U-Pb dating by LA-ICP-MS was set to 20  $\mu\text{m}$  (30  $\mu\text{m}$  pre-ablation), using the GJ1 reference zircon (Boekhout et al., 2012; Ulianov et al., 2012) for the standardization of relative sensitivity factors and Plešovice (Sláma et al., 2008) as a secondary standard for accuracy control. The SIMS was operated at a beam size of  $10 \times 8$   $\mu\text{m}$ , using Temora (Black et al., 2004) and Plešovice (Sláma et al., 2008) standards. Trace elements were analyzed for selected samples by LA-ICP-MS, setting different spot diameters depending on the size of the target zircon domain (50, 38, or 30  $\mu\text{m}$ ), and using the SMR612 and BCR-2G glass standards.

Data reduction for LA-ICP-MS analyses was performed using Lamtrace software (Jackson, 2008). As an additional control of the spot positions, zircon populations were subjected to an a posteriori CL-check. The craters ablated on more than one growth zone, on densely fractured spots, or with inclusions were not further considered. Finally, the data were plotted on a Wetherill Concordia diagram using IsoplotR (Vermeesch, 2018). All the graphically discordant analyses were avoided from the Concordia age calculations. Zircon dates in the text are LA-ICP-MS dates, indicated as Concordia ages with a  $2\sigma$  confidence interval, unless otherwise specified (e.g., SIMS dates).

The complete description of the applied methodology is reported in Supporting Information S1 (*Methodology.docx*).

Furthermore, in Supporting Information S1 *Maps\_extended.pdf*, there are the extended versions of Figures 3–5 with geological maps and sections, together with the relevant stereographic projections of structural data. The detailed mineralogy of all sampled rocks is summarized in Table 1 and the relevant detailed thin section descriptions can be found in *THINSECTIONS\_description.docx*. The measured U-Pb zircon data are reported in Supporting Information S1 *UPb\_LAICPMS folder* and *UPb\_SIMS.xlsx*, respectively for LA-ICP-MS and SIMS analyses, whereas the results of geochemical analyses are in *Trace\_LAICPMS.xlsx*. LA-ICP-MS data distribution for all samples is represented in Kernel Density Estimates in Supporting Information S1 *KDE\_LAICPMS.pdf*, computed with IsoplotR (Vermeesch, 2018). Discordia lower intercepts for SIMS analyses calculated in the Tera-Wasserburg diagram are in *Tera-Wasserburg\_SIMS.pdf*, also computed with IsoplotR (Discordia Model-1; Vermeesch, 2018). Analytical results and Concordia diagrams for reference materials adopted in LA-ICP-MS analyses are in *Stds\_LAICPMS.xlsx*.

## 4. Geological Results and Zircon Growth: Structural Position, Sample Description, Zircon CL-Images, U-Pb Ages, and Geochemistry

### 4.1. The Cima di Gagnone Area

In the mapped area (Figure 3), the Cima Lunga unit lies above orthogneisses, minor paragneisses and amphibolites of the Simano nappe. The Cima Lunga unit consists of biotite-muscovite paragneisses and micaschists, locally garnet-bearing, that wrap lenses of garnet peridotite and chlorite harzburgite. The metasedimentary stratigraphy is locally interlayered with amphibolites, which are locally boudinaged, and by quartzo-feldspathic gneisses

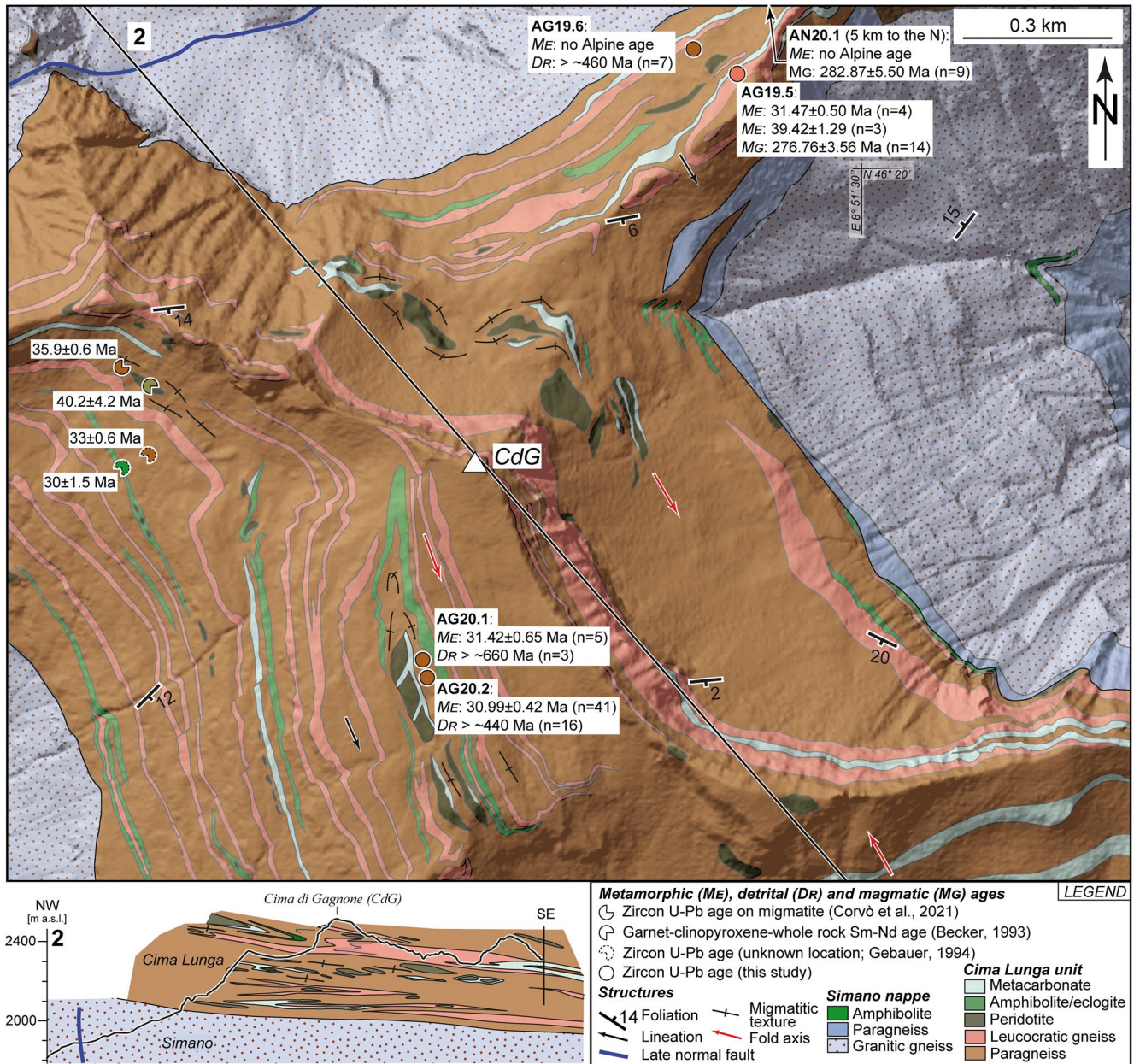


**Figure 3.** Geological-structural map of the first studied area, Cima di Gagnone, with the relevant geological section (*Profile 2*) (with minor modifications after Corvò et al. (2021) and Pfiffner and Trommsdorff (1997)). The ages of samples from this study and literature data are indicated in the map. Notice the continuity of lithotypes and the boudinage of ultramafics in the Cima Lunga unit. The zircon U-Pb ages from this study indicated in this map are LA-ICP-MS ages. An extended version of this figure is in Supporting Information S1 *Maps\_extended.pdf*.

(Figure 3; AG19.5) of unknown protolith. Ultramafics are typically structurally linked with metacarbonates, being wrapped by and deformed together with them, and include basaltic amphibolites, eclogites, metaroddingites and eclogitic metaroddingites.

In the Cima Lunga unit, the presence of sheath folds documents highly sheared zones within a general top-to-NW shearing sense, as also previously documented by asymmetric sigmoids and garnet rotation (see also structural details in Maino et al. (2021)). The transition from the Simano nappe up to the contact with the Cima Lunga unit is marked by an overall progressive (but locally not linear) change in the gneiss texture, parallel to the regional foliation. The fabric is more developed toward the top of the sequence over ca. 200 m (e.g., decreased grain size, elongated lithons), suggesting an upward strain increase in the direction of the Cima Lunga unit. On the regional foliation plane, the penetrative lineation trends NW-SE.

The HP/HT assemblages of mafic/ultramafic lenses are largely overprinted by amphibolite facies assemblages, which also dominate the enveloping paragneiss host rocks. Migmatitic structures occur around the ultramafic bodies as stromatic leucosomes and locally in the paragneisses as leucocratic intrafoliation pockets boarded by a melanocratic rim (Figures 2a and 3; AG20.1, AG20.2). This sporadic incipient melting is more prominent around the ultramafic inclusions and the volumes of partial melting in the Cima Lunga unit is visually estimated in the field to maximal 2–3 vol%. Syn- to post- (Alpine) foliation veins containing quartz, kyanite and andalusite suggest that a release of fluids from the paragneisses occurred late in the decompression history (at  $P \leq 0.4$  GPa), but still at 600–675°C, as also previously noted and computed by Allaz et al. (2005).

**Quartzo-feldspathic gneiss AG19.5** was sampled in the Cima Lunga unit from a continuous gneissic horizon located above metacarbonates and ultramafic lenses, and below paragneisses (Figure 3). The rock texture is granoblastic with sparse feldspar augen. Foliation is defined by the preferred orientation of quartz, feldspar, biotite and white mica. Elongated mica flakes and quartz and feldspar aggregates define the lineation. At the micro-scale, grain boundary migration, subgrain rotation and myrmekites of feldspars and quartz suggest dynamic recrystallization at temperatures above 500°C (Passchier & Trouw, 2005; Stipp et al., 2002).

Rimmed zircon cores display a non-unique appearance in CL images (Figure 6), reflected in a wide range of dates. Zircon core dates are spread along the Concordia line (total number of concordant analyses is  $n = 31$ ): the oldest are ca. 1000 Ma ( $n = 2$ ), a population is between 700 Ma and 400 Ma ( $n = 15$ ), and the highest density cluster is at  $276.76 \pm 3.56$  Ma (Concordia age;  $n = 14$ ; MSWD = 1.3; Figure 7). This Permian population is composed of both oscillatory cores and faint oscillatory rims around older cores (Figure 6), and it shows Th/U ratios tendentially higher than 0.1 (median value: 0.339; Table 1), indicative of magmatic zircon (Hoskin & Schaltegger, 2003; Teipel et al., 2004). The magmatic Th/U ratios, the oscillatory growth around older zircon grains, and the orthogneissic texture of the rock advocate a Permian magmatic age of the rock. Finally, rare homogeneous CL-gray rims wrap the zircon grains, giving dates split in two groups at  $39.42 \pm 1.29$  Ma (Concordia age;  $n = 3$ ; MSWD = 12) and  $31.47 \pm 0.50$  Ma (Concordia age;  $n = 4$ ; MSWD = 9.6) (Figure 8). Their Th/U is between 0.001 and 0.040 (Table 1), typical of metamorphic zircon (Teipel et al., 2004).

**Quartzo-feldspathic gneiss AN20.1** was sampled in Val Nédro (north of Figure 3), at the base of the Cima Lunga unit. Foliation is defined by biotite, partially replaced with chlorite, and there is a large variability in lithons' composition: facies having feldspar augen and quartz-rich facies can both be found at the meso-scale. In thin section we observe that pre-existing feldspar augen can be replaced by newly-formed plagioclase grains and myrmekites along their boundaries, pointing to recrystallization temperatures above 500°C (Passchier & Trouw, 2005).

Cathodoluminescence images depict zircon cores with oscillatory or sector zoning rimmed by a discordant oscillatory zone. Three cores resulted in dates between ca. 420 and 590 Ma, whereas nine other cores and oscillatory rims formed a cluster at  $282.87 \pm 5.50$  Ma (Concordia age;  $n = 9$ ; MSWD = 0.63; Figure 7). Zircon cores have Th/U > 0.45, and zircon rims Th/U < 0.05 (Table 1) in the range of metamorphic zircon (Teipel et al., 2004). The within-error coeval magmatic cores and magmatic/metamorphic oscillatory rims coupled with the overall texture of the rock hint at a quartz-rich magmatic protolith of  $282.87 \pm 5.50$  Ma age.

**Garnet-paragneiss AG19.6** was sampled above calcschists and leucogneisses, and below ultramafic lenses (Figure 3). It is characterized by cm-scale pre- to syn-tectonic snowball garnets and a tectonic fabric defined by kyanite and biotite with a preferred orientation, also defining the mineral lineation. Grain boundary migration microstructures indicate quartz and feldspar dynamic recrystallization.

Two main groups of dates at ca. 585 Ma and ca. 460 Ma were detected for magmatic oscillatory and sector-zoned cores (Figure 6). SIMS gave a date of  $468.4 \pm 13.4$  Ma ( $n = 1$ ; Pb<sup>206</sup>/U<sup>238</sup> age; error 2 $\delta$ ; see Supporting Information S1 *UPb\_SIMS.xlsx*) for a magmatic core (Th/U = 0.38). A thin metamorphic rim (Th/U = 0.02), homogeneous, CL-gray in color and sub-idiomorphic, yields an age of  $322.9 \pm 30.4$  Ma ( $n = 1$ ; Pb<sup>206</sup>/U<sup>238</sup> age; error 2 $\delta$ ; *UPb\_SIMS.xlsx*), indicative of Carboniferous metamorphism. Therefore, the magmatic dates likely belong to detrital zircon grains and the deposition age of these metasediments predates the Variscan orogeny.

*Migmatitic garnet-paragneiss AG20.1* was sampled above an HP ultramafic lens at Cima di Gagnone (Figure 3). At the meso-scale, the rock has leucocratic migmatitic intra-foliation layers. The thin section shows that both biotite and white mica define the foliation and garnets are pre- to syn-kinematic. Some garnets are at the borders of the leucocratic domains.

Zircon cores display oscillatory zoning, dated at  $687.09 \pm 23.82$  Ma (Concordia age;  $n = 3$ ; MSWD = 3.3) and a Th/U between 0.09 and 1.00 (Table 1). CL-gray rims, usually thick, with a smooth zoning pattern, wrap the zircon (Figure 6). Their dates are clustered at  $31.42 \pm 0.65$  Ma (Concordia age;  $n = 5$ ; MSWD = 3.7; Figure 8) and they have a metamorphic Th/U imprint (0.005–0.007; Table 1; Teipel et al., 2004). In these rims, the positive Ce-anomaly, the absence of the Eu-anomaly and the flat HREE profile (Figure 9) together suggest zircon growth from incipient anatectic melt (Sawyer, 2008) in the presence of garnet (e.g., Rubatto, 2002), placing the migmatization at  $31.42 \pm 0.65$  Ma.

*Migmatitic garnet-paragneiss AG20.2* was collected in a rock portion with leucocratic cm-scale pockets (Figure 2a). Leucosomes boarded by melanosomes also occur as boudinaged intrafoliation lenses, locally folded. Garnets are pre- to syn-kinematic, and quartz is more abundant with respect to feldspar. Undulose extinction of feldspars and quartz, coupled with the preferred orientation of quartz aggregates, indicate dynamic recrystallization.

Zircon cores have magmatic oscillatory or sector zoning, sometimes with rounded or zoning-parallel inclusions (Figure 6). Their Concordia age is  $548.76 \pm 10.57$  Ma ( $n = 16$ ; MSWD = 4.5), associated with magmatic Th/U of 0.22–0.87 (Table 1). Abundant metamorphic layers with chaotic zonation and ubiquitous rounded inclusions (generally <ca. 10  $\mu\text{m}$ , up to ca. 20  $\mu\text{m}$  in diameter) grew outside the cores (Figure 6). Two inclusion-free spots gave concordant dates at  $315.30 \pm 16.71$  Ma (Concordia age;  $n = 2$ ; MSWD = 1.0). Finally, thick metamorphic rims (up to ca. 30–35  $\mu\text{m}$ ) with low Th/U ratios (0.001–0.010; Table 1) wrapping the zircon have an age of  $30.99 \pm 0.42$  Ma (Concordia age;  $n = 41$ ; MSWD = 17; Figure 8). Similar to *AG20.1*, the absence of the Eu-anomaly accompanied by a positive Ce-anomaly and a flat HREE profile indicate zircon growth while garnet and incipient anatectic melt coexisted (Figure 9), pointing to a partial melting event at  $30.99 \pm 0.42$  Ma.

#### 4.2. The Cima di Precastello Area

In this mapped area (Figure 4), the Cima Lunga unit is sandwiched between orthogneisses that are attributed to the Simano nappe. The Cima Lunga unit is constituted by an intensely folded sequence of paragneisses, leucocratic gneisses and metacarbonates, mainly calcschists. East of the mountain ridge of Cima di Precastello, these calcschists can be continuously followed over 6–10 km to the south (Figure 1). The stratigraphy of the bottom part of the Cima Lunga unit alternates calcschists with amphibolitic paragneisses, and local layers of a quartzo-feldspathic gneiss whose protolith nature and age are unknown (*AN19.6*). At the top of the Cima Lunga unit, paragneisses are interfingering by Simano orthogneisses, that are locally folded (Figure 4). Here, the orthogneisses show sporadic migmatitic textures. The whole package is overlaid by granitic to dioritic orthogneisses that are diagnostic for the Maggia nappe (Rüscada and Cocco gneisses; Bussien et al., 2011). At the base of the Maggia nappe, migmatites with stromatic patches and a complex deformed network of leucosomes (Figure 2c; *OS17-013*) testify partial melting during deformation. The contact is folded, having a fold axis parallel to the NW-SE directed lineation. On planes orthogonal to the lineation, these folds depict concentric- or  $\Omega$ -shapes typical of sheath folds (see *Profile 4* in Figure 4), reflecting a high non-coaxial strain along the tectonic contact at the base of the Maggia nappe.

According to the mineral assemblages, we consider the metamorphic conditions in this area similar to those described in the Cima di Gagnone area, even though no eclogite was found and no detailed petrological study has been published.

*Quartzo-feldspathic gneiss AN19.6* was sampled at the base of the Cima Lunga unit to the east (Figure 4), in between metacarbonate layers. The tectonite fabric is defined by quartz-feldspar lithons and films of biotite and white mica. In the foliation, abundant feldspathic millimetric to centimetric augen with elliptical shape (Figure 2b) indicate a magmatic protolith. The thin sections show evidence of crystal lattice distortion and dynamic recrystallization in the rock, such as undulose extinction, subgrain rotation in quartz and feldspars, and grain boundary migration in quartz (only a few cases in feldspar), but also myrmekites, which indicate temperatures above ca. 500°C (Passchier & Trouw, 2005).

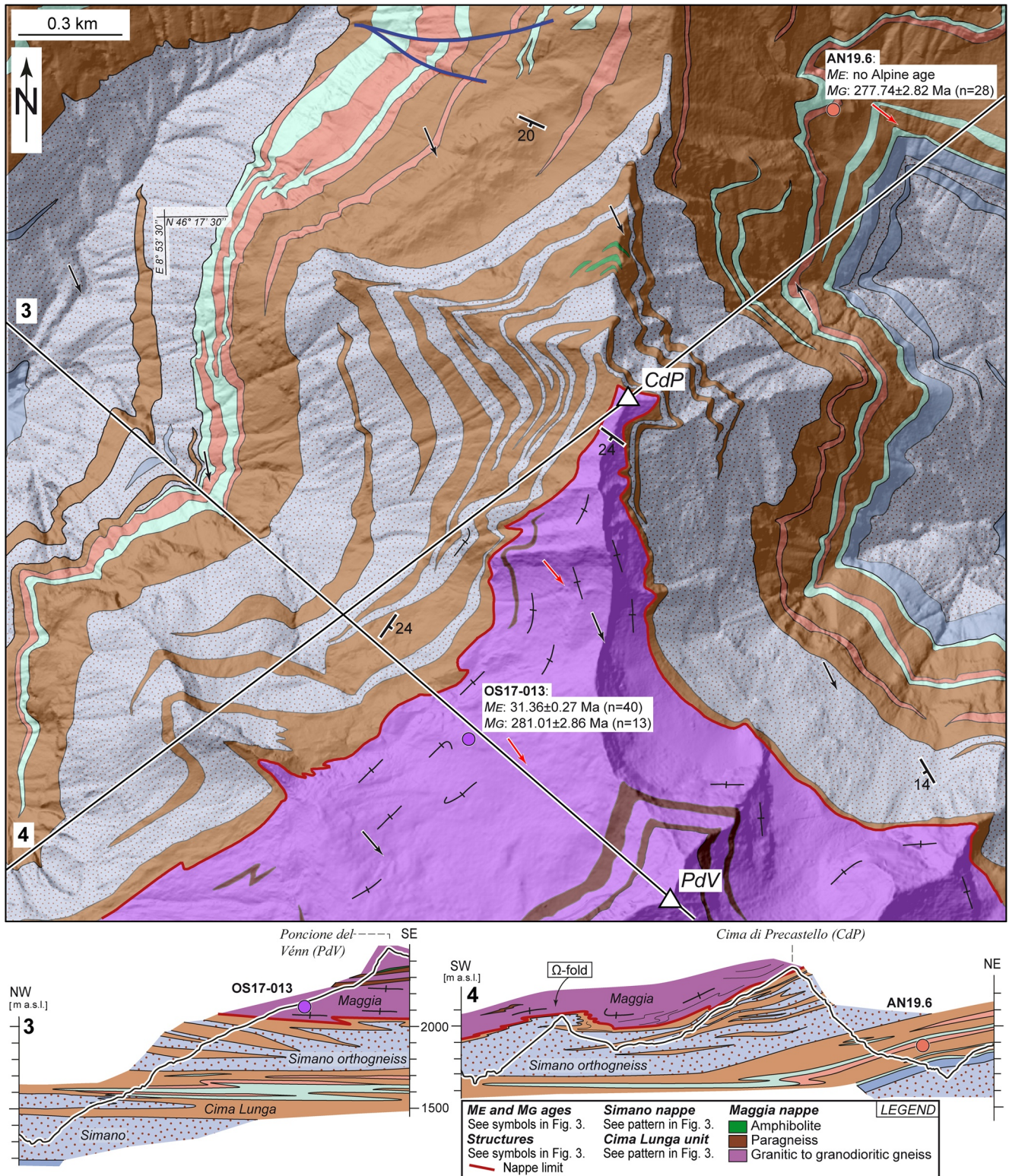


**Figure 4.** Geological-structural map of the second studied area, Cima di Precastello, with the relevant geological sections (*Profile 3, 4*). Own samples and LA-ICP-MS U-Pb zircon ages are indicated in the map. An extended version of this figure is in Supporting Information *S1 Maps\_extended.pdf*.

Zircon crystals are formed by an outer irregular, extremely thin (ca. 5  $\mu\text{m}$ ) rim wrapping the cores. Only in a few cases were these rims wide enough to analyze, although they yielded discordant dates. The inner part of the zircon cores is mostly idiomorphic, with oscillatory zoning, typical of magmatic zircon. However, the outermost layers of the core are typically damaged or resorbed, resulting in a porous aspect, or sometimes show damage trend parallel to the oscillatory zoning (Figure 6). The  $\text{U}^{238}$  content of the porous zircon zones is higher than that of the pristine cores (5,535 ppm and 1,053 ppm respectively; see *Trace\_LAICPMS.xlsx*). In some cases, the boundary between the apparently undamaged and the damaged zircon portions is gradational. Spot analyses of damaged zones resulted in discordant dates. On the same oscillatory cores we could observe younger dates from the innermost portion of the zircon at  $277.74 \pm 2.82$  Ma (Concordia age;  $n = 28$ ; MSWD = 1.6; Figure 7) to the parts closer to the damaged zones (until ca. 220 Ma old; see distribution in *KDE\_LAICPMS.pdf*), with Th/U ratios for the pristine cores between 0.15 and 0.72 (Table 1). These considerations and the orthogneissic texture of the rock point to a magmatic protolith, whose intrusion age is close to the age of the inner undamaged zircon at  $277.74 \pm 2.82$  Ma.

**Migmatitic orthogneiss OS17-013** was sampled from a leucosome-rich fraction of the migmatitic portion (metatexite to diatexite) of the Ruscada orthogneiss along the contact between the Maggia nappe with the lower rocks of the Cima Lunga unit and Simano nappe (Figure 4). At the outcrop scale (Figure 2c), the structures of the migmatites can be variable ranging from a layer-structured (in most cases) to local net-structured metatexites where both in situ and in-source leucosomes can be seen (see Sawyer, 2008 as reference for migmatites' description). Some leucocratic portions are folded, and in a few cases a local patchy morphology can be seen. The rock consists of biotite, white mica, elongated and platy quartz and feldspar aggregates forming the foliation, with evidence of incipient melting at the micro scale which is testified by for example, polysynthetic twinning in plagioclase (Vance, 1961), and possibly indicated by tartan pattern in feldspars (Winter, 2013).

The oscillatory and sector-zoned zircon cores (Figure 6) are dated at  $281.01 \pm 2.86$  Ma (Concordia age;  $n = 13$ , MSWD = 2; Figure 7) with most Th/U ratios in the magmatic range (0.06–0.33; Table 1). The cores are surrounded by outer layers that are not considered for magmatic age calculation being resorbed or with complex zoning patterns. The outermost layer has a very low Th/U (0.0006–0.009; Table 1) pointing to a metamorphic origin (Teipel et al., 2004) and migmatization age at  $31.36 \pm 0.27$  Ma (Concordia age;  $n = 40$ , MSWD = 0.71; Figure 8).

### 4.3. The San Vittore-Giova Area

In the San Vittore-Giova area (Figure 5), the Adula nappe rests above the Simano nappe. The Simano nappe consists of leucocratic orthogneisses with porphyroblastic biotite, forming a large body that extends for several kilometers to the north and to the east. Minor volumes of paragneisses, locally containing garnets, and amphibolite lenses crop out above and inside this body. All along the upper tectonic contact of the Simano nappe with the Adula nappe, the orthogneisses and paragneisses show diffuse migmatitic textures (Figures 2e–2g; AV19.3, AV19.4, AV19.7) which are locally transected by granitic dikes (Figures 2g and 2h; AV21-001, AV21-002). The migmatitic texture disappears downsection in the tectonostratigraphy. The base of the Adula nappe is dominated by paragneisses and micaschists of the Salahorn formation (Cavargna-Sani, Epard, & Steck, 2014) and minor layers of orthogneisses. These rocks contain abundant stretched and folded intra-foliation quartz-veins. During deformation, the fluids that precipitated within these veins increased the mica content of the rocks which makes the macroscopic distinction between ortho- and para-gneisses difficult. In these gneisses, we do not observe migmatitic textures.

The roof of the Simano nappe is formed by a 200–400 m thick sequence that alternates paragneisses, micaschists, marbles, metaconglomerates and leucogneisses. The paragneisses and quartzo-feldspathic gneisses show (at least at the base) migmatitic textures. The origin and the tectonic attribution of this folded and stretched sequence are unknown. The planes of alternating lithotypes and rock foliation dip to the southeast with an angle that gradually changes southwards from ca. 30° to ca. 60°, depicting the bending of the tectonostratigraphy in the SSB (*Profile 5* in Figure 5). In this sequence of San Vittore, south-vergent asymmetric folds have SE plunging fold axis parallel to the mineral and stretching lineation (Figure 5). The upper limbs are often sheared in a top-to-NW direction. This shearing occurred close to peak  $T$  metamorphic conditions and was the dominant deformation regime, as deduced from shear bands containing migmatitic leucosomes (Figures 2f and 2g; AV19.3, AV19.4), sigma clasts (Figure 2d; AV19.1) and rotated garnets (Figure 2e; AV19.7) all over the studied area.

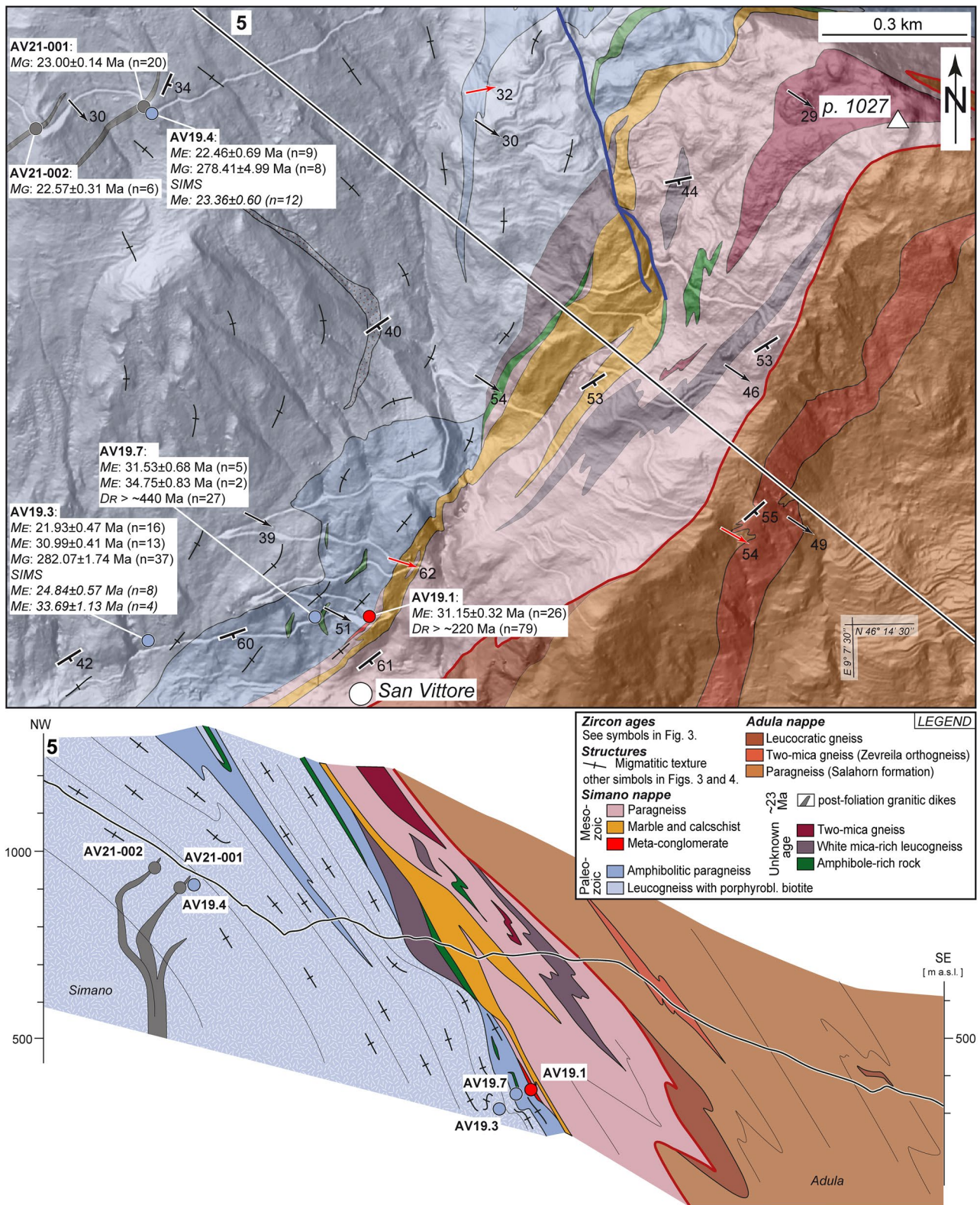


**Figure 5.** Geological-structural map of the third studied area, San Vittore-Giova, with the relevant geological section (*Profile 5*). Own samples and U-Pb zircon ages are indicated in the map. If not specified, zircon U-Pb ages are LA-ICP-MS ages. An extended version of this figure is in Supporting Information [S1 Maps\\_extended.pdf](#).

In the studied area, the metamorphism of the Simano nappe reached partial melting conditions ( $\geq$ ca. 650°C). Structurally below the migmatites, 5 km to the north, the peak conditions of the Simano nappe were computed at ca. 600°C and 0.4 GPa (Rütti, 2001), whereas peak  $T$  conditions in the Adula nappe were estimated around 700°C during decompression until 0.6–0.8 GPa (Nagel et al., 2002; Rütti et al., 2008).

**Quartzo-feldspathic gneiss AV19.1** is a metaconglomerate, with centimetric, elliptical augen made of quartz and feldspar (Figure 2d). Folded veins, locally quartz-rich, lay within the foliation, defined by the preferred orientation of biotite. At the micro-scale, polysynthetic twinning in plagioclase and growth of fine-sized lobate quartz crystals from plagioclase borders testify incipient partial melting (Paterson et al., 1989). Zircon grains have a heterogeneous morphology and internal zonation (Figure 6). Zircon cores also show variability in the inclusion content (Figure 6): (a) CL-dark gray inclusion-rich inner cores surrounded by a CL-gray layer, and (b) CL-light gray to gray inclusion-free cores. Their dates are spread along the Concordia over 1000 Ma, with the highest density of analyses around 300 Ma (Figure 7) and the second highest at 600–650 Ma. Th/U is usually higher than 0.1 (max. 1.73; Table 1), even though some Permo-Carboniferous cores show lower values (min. 0.002; Table 1). The distribution of concordant dates ranges from Precambrian to Permian-Triassic (Figure 7; see *KDE\_LAICPMS.pdf* in Supporting Information S1). Finally, zircon cores are wrapped by CL-dark gray metamorphic rims, dated at  $31.15 \pm 0.32$  Ma (Concordia age;  $n = 26$ ; MSWD = 24; Figure 8), and having low Th/U ratios (0.001–0.015; Table 1). We attribute this age to the beginning of partial melting at the micro-scale, hence to the migmatization stage. The morphological-heterogeneous population of the detrital cores (Figure 6) and the spreading of concordant dates down to ca. 180 Ma (Figure 10) suggest a Mesozoic deposition age.

**Migmatitic garnet-paragneiss AV19.7** has cm-scale pre- to syn-tectonic garnets and shows mylonitic to migmatitic fabric (Figure 2e) identified by the preferred orientation of biotite, which also defines the mineral lineation. Locally, at the meso-scale, asymmetric leucocratic pockets show a top-to-NW shear sense and migmatization. At the micro-scale, two main stages of garnet fabric evolution can be identified: (a) nucleation and growth prior to the development of the main tectonic foliation, and (b) growth within the biotite + quartz + feldspar + kyanite foliation, associated with partial melting (see thin sections description in Supporting Information S1: *THINSECTIONS\_description.docx*).

Zircon grains have magmatic oscillatory or sector-zoned cores, anhedral in shape, sometimes eroded (Figure 6), with dates spanning between ca. 475–625 Ma. Metamorphic rims are present. Some of them have dates around ca. 300 Ma. The outermost metamorphic rims with low Th/U ratios (0.002–0.009; Table 1) cluster at  $34.75 \pm 0.83$  Ma (Concordia age;  $n = 2$ ; MSWD = 0.86) and  $31.53 \pm 0.68$  Ma (Concordia age;  $n = 5$ ; MSWD = 0.46) (Figure 8). Similar to the Cima Lunga migmatitic paragneisses (*AG20.1*, *AG20.2*), the Ce-anomaly, the absence of Eu-anomaly, and flat HREE profile (Figure 9) reflect zircon crystallization in coexistence of incipient anatectic melt and garnet growth (Sawyer, 2008), prior to plagioclase crystallization (e.g., Rubatto et al., 2009) or with Eu-depleted plagioclase (e.g., Gregory et al., 2009). The  $34.75 \pm 0.83$  Ma zircon rims have slightly lower HREE hinting at a metamorphic/migmatitic precursor involving garnet growth coeval with zircon formation. SIMS analyses gave one concordant date at  $32.9 \pm 1.0$  Ma ( $n = 1$ ;  $\text{Pb}^{206}/\text{U}^{238}$  age; error 2 $\sigma$ ; Figure 8).

**Migmatitic orthogneiss AV19.3** was sampled from a leucocratic portion of the rock. The rock texture is formed by mica films (biotite and white mica) and quartz-feldspar lithons, many of which gradually transition into leucocratic melt pockets, which locally accumulate in stromatic leucosomes parallel to the foliation, or within shear bands, or in veins cutting the foliation. Leucosomes may be locally folded, giving an overall picture of a syn-tectonic migmatite.

Zircon grains have inclusion-rich magmatic cores with oscillatory or sector zoning, their age is  $282.07 \pm 1.79$  Ma (Concordia age;  $n = 37$ ; MSWD = 1; Figure 7) and Th/U ratios cluster at ca. 0.4 (Table 1). The cores are wrapped by partially resorbed layers showing a pattern of porous, convoluted zones, CL-black, frequently with cavities filled by later CL-gray zircon growth (Figure 6). Finally, the outermost layers are metamorphic rims showing multiple growths. The inner ones are typically CL-gray and thick, with low Th/U ratios (median value: 0.004; Table 1) and an age of  $30.99 \pm 0.41$  Ma (Concordia age;  $n = 13$ ; MSWD = 5.1; Figure 8). Outside, several thin layers (inner CL-light gray, outer CL-black) yielded an age of  $21.93 \pm 0.47$  Ma (Concordia age;  $n = 16$ ; MSWD = 1.1; Figure 8), having also low Th/U ratios (0.001–0.114; Table 1). We also analyzed the zircon rims using SIMS, and they were dated at  $33.69 \pm 1.13$  Ma (Concordia age;  $n = 4$ ; MSWD = 3.7) and  $24.84 \pm 0.57$  Ma (Concordia age;  $n = 8$ ; MSWD = 0.46) respectively (Figure 8). The REE profile of the  $30.99 \pm 0.41$  Ma zircon



**Figure 6.** Cathodoluminescence (CL) images of representative zircon crystals. The big circles represent the LA-ICP-MS spot analyses (20 or 30 μm diameter), whereas the smaller elliptical ones indicate the SIMS spots (8 × 10 μm). The reported dates are  $^{206}\text{Pb}/^{238}\text{U}$  (Ma) ± 2 sigma error. See the text for discussion on zircon internal stratigraphy and relevant ages.

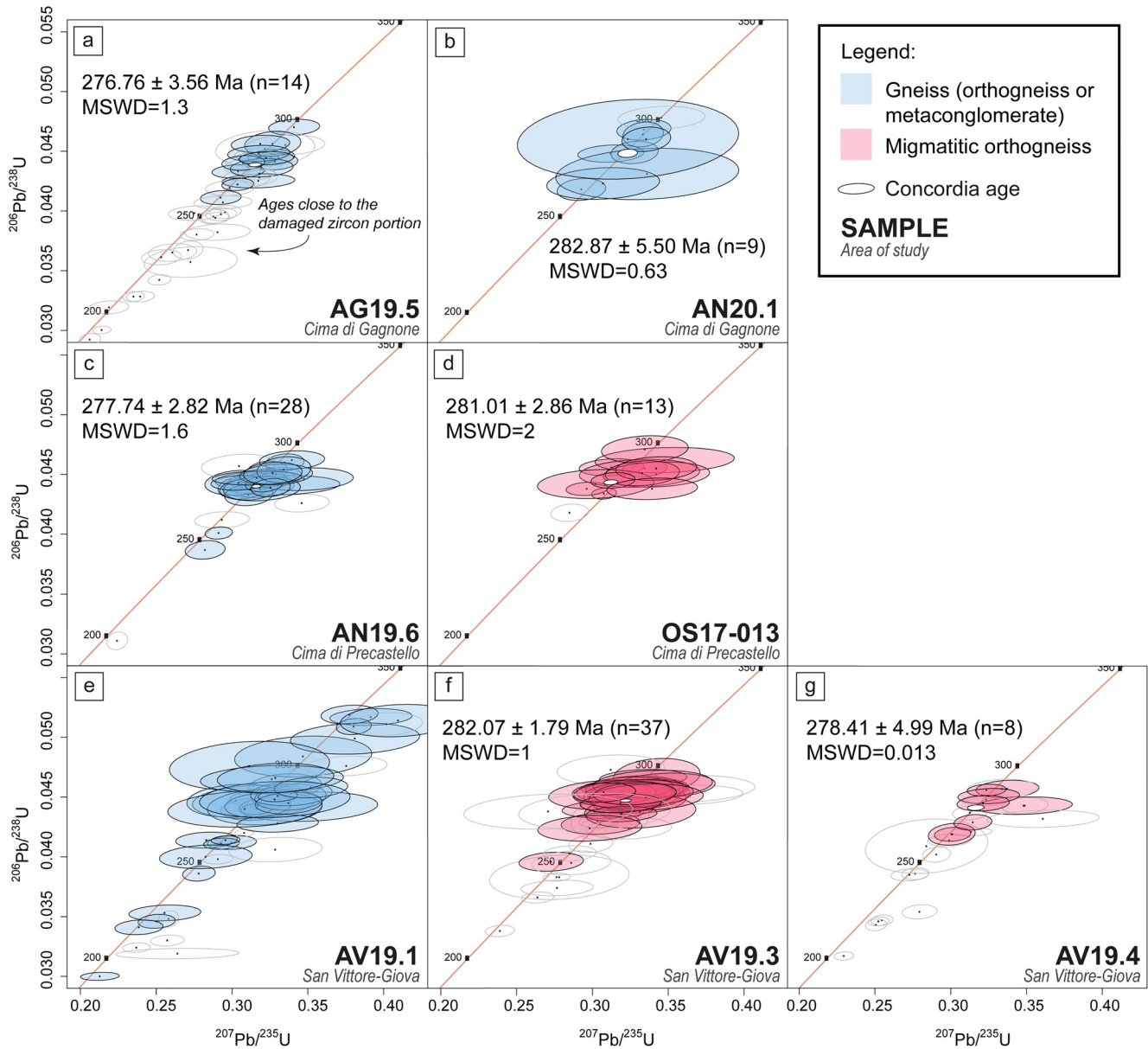


**Figure 7.** Wetherill Concordia plots for Permian ages. The age estimates are Concordia ages computed using IsoplotR (Vermeesch, 2018), and the mean square of weighted deviation (MSWD) is also calculated (both are absent in panel (e)). The number of concordant analyses considered for the calculation is indicated in brackets ( $n$ ). Colorless ellipses represent discarded data. In panel (e): zoom of data distribution for detrital zircon grains in sample AV19.1, no age is computed.

population has a positive slope with high HREE contents and Eu-negative and Ce-positive anomalies (Figure 9), possibly formed during zircon crystallization in the absence of garnet in evolved melts where a substantial amount of plagioclase was already crystallized (Sawyer, 2008). Trace element measurements were not performed on the outer younger rims because of their insufficient thickness.

**Migmatitic orthogneiss AV19.4** was sampled from leucocratic portions of the rock along the same migmatitic belt of AV19.3. Its morphology is predominantly stromatic with veins or pockets cutting the foliation. Frequent dm-scale shear zones with melt in the shear plane (Figure 2g), coupled with the asymmetric shape of some cm-scale melt pockets, indicate a top-to-NW shear sense parallel to the pervasive mineral lineation visible on the foliation planes.

Zircon internal stratigraphy is analogous to AV19.3. CL-gray cores provide an age of  $278.41 \pm 4.99$  Ma (Concordia age;  $n = 8$ ; MSWD = 0.013; Figure 7). These inner cores transition to damaged or resorbed layers with

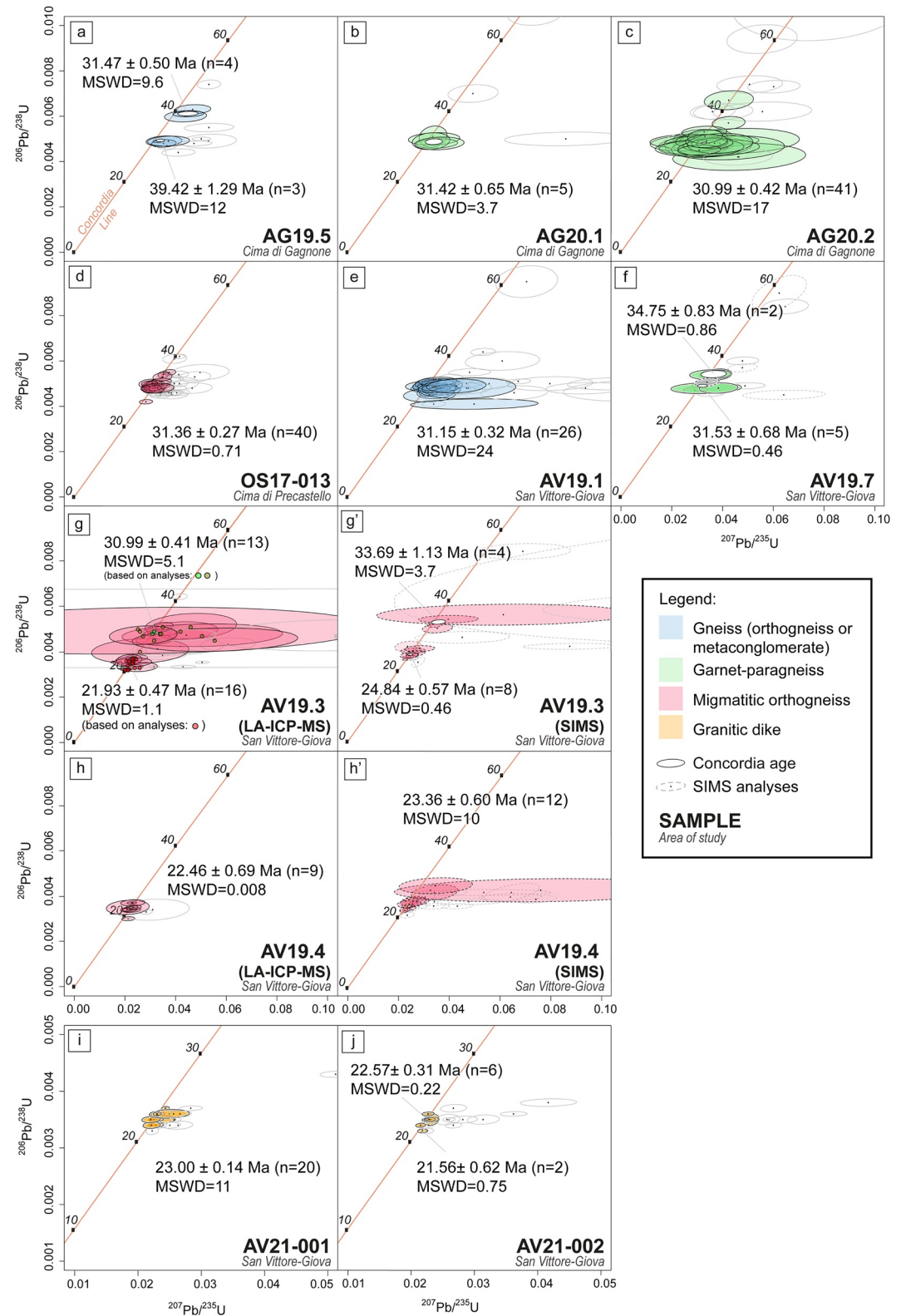


**Figure 8.** Wetherill Concordia plots for Alpine ages. Concordia ages are computed using IsoplotR (Vermeesch, 2018); the number of concordant analyses considered for the calculation is indicated in brackets ( $n$ ) and is represented by color-filled ellipses. LA-ICP-MS data points are indicated with solid lines and SIMS results with dashed lines. For comparison, SIMS data computed with IsoplotR Discordia Model-1 (Vermeesch, 2018) in the Tera-Wasserburg diagram are reported in Supporting Information S1 Tera-Wasserburg\_SIMS.pdf.

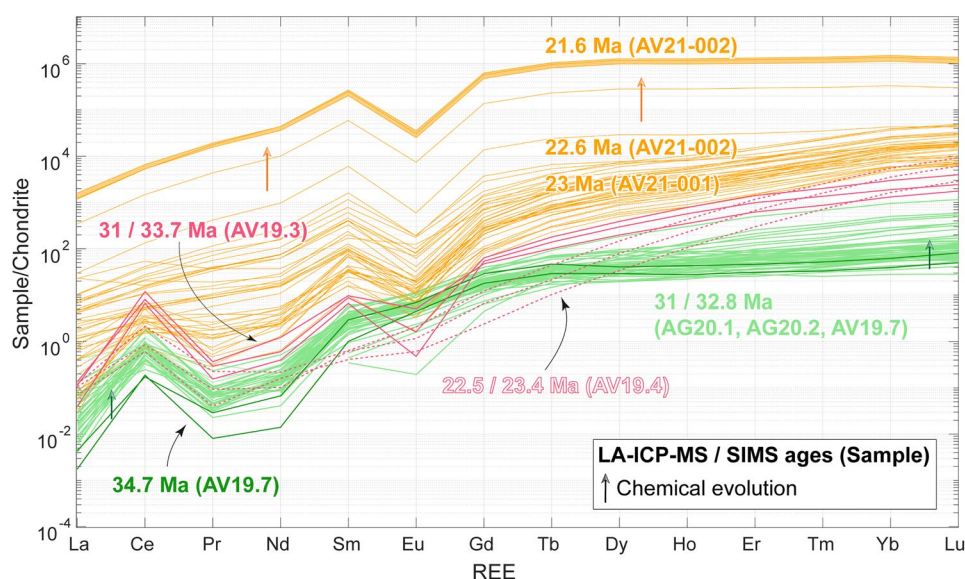


**Figure 9.** REE chondrite-normalized patterns for different samples (the same colors used in the precedent figures correspond to the different lithotypes). Trace element abundances were measured with LA-ICP-MS in the same zircon domains analyzed for U-Pb zircon dating (see main text for discussion). All the analyses are reported in Supporting Information *S1 Trace\_LAICPMS.xlsx*.

porous structure toward the external portions of the zircon, which are ultimately wrapped by metamorphic rims (Figure 6). The outermost layer of rims we already identified in sample AV19.3, the CL-light gray and CL-black rims, is more developed in this sample. The age of these rims resulted in  $22.46 \pm 0.69$  Ma (Concordia age;  $n = 9$ ; MSWD = 0.0079) for LA-ICP-MS and  $23.36 \pm 0.60$  Ma (Concordia age;  $n = 12$ ; MSWD = 10) for SIMS analyses (Figure 8). Th/U ratios cluster at ca. 0.5 for inner cores, whereas they are lower for the rims (median value: 0.006; Table 1). Rims' REE pattern is marked by a positive slope with low MREE, no Eu-negative anomaly and a less pronounced Ce-anomaly compared to the analyzed metamorphic rims of sample AV19.3. This evidence suggest zircon rim crystallization during metasomatism or hydrothermalism (e.g., Fu et al., 2008; Geisler et al., 2003, 2007; Hoskin, 2005; Hoskin & Black, 2000).

**Granitic dike (pegmatite) AV21-001** was sampled from a pegmatitic dike cutting sharply across the migmatitic foliation of sample AV19.4 (Figure 2g). It contains quartz, feldspar, porphyroblastic biotite, and locally (unzoned, Ca-poor) garnet. Zircon grains have complex internal stratigraphy showing convoluted zoning and patchy patterns of CL-black and CL-gray zones (Figure 6). Their age is  $23.00 \pm 0.14$  Ma (Concordia age;  $n = 20$ ; MSWD = 11; Figure 8). The low Th/U ratios are unusual for magmatic zircon crystals (0.0003–0.013; Table 1). The U content is high (average of 19,866.24 ppm for  $^{238}\text{U}$ ; see *Trace\_LAICPMS.xlsx* in Supporting Information S1). REE contents are high, reaching values of  $10^3$ – $10^4$  higher than chondritic for Lu, with Eu-negative anomaly but not always showing a Ce-positive anomaly (Figure 9), hence suggesting zircon crystallization in variable oxygen fugacity conditions (Hoskin & Schaltegger, 2003).

**Granitic dike (aplite to pegmatite) AV21-002** is an approximately 40 cm thick dike showing both pegmatitic (central part) and aplitic portions (Figure 2h). It contains quartz, feldspar with porphyroblastic biotite, and locally garnet. At the micro-scale, the fabric is magmatic. However, also small deformation signs can be observed, such as deformation lamellae in plagioclase or local slight kinking of white mica. Zircon grains show patchy CL-patterns (Figure 6). Their age is  $22.57 \pm 0.31$  Ma (Concordia age;  $n = 6$ ; MSWD = 0.22; Figure 8), they have low Th/U ratios (0.003–0.004; Table 1), and REE content covering a wide range, with Lu abundances  $10^4$ – $10^5$  higher than chondritic (Figure 9). The flat HREE profile, the Eu-negative anomaly, and the absence of Ce-anomaly (Figure 9) hint at zircon crystallization under reducing conditions (Hoskin & Schaltegger, 2003). Late zircon overgrowths, CL-dark gray to black in color, appear as a triangular protuberance grown on top of a pre-existing zircon (Figure 6), and have an age of  $21.56 \pm 0.62$  Ma (Concordia age;  $n = 2$ ; MSWD = 0.75; Figure 8). These overgrowths also have low Th/U ratios (ca. 0.06; Table 1) and the REE trend is similar to that of the other zircons, although at higher abundances, reaching values of  $10^6$  higher than chondritic for Lu (Figure 9).

For this sample, from the REE evolution and from the aplitic to pegmatitic texture, we can suggest that the dike intruded at  $22.57 \pm 0.31$  Ma and that around  $21.56 \pm 0.62$  Ma late fluids/melts were still percolating within it.

## 5. Discussion

### 5.1. Methodological Considerations on Zircon U-Pb Dating

We recognized three main zircon domains (Figure 6) in the lithotypes of the Lepontine dome (Figure 10): (a) pre-Permian detrital or Permian magmatic cores (Figure 7), (b) intermediate porous layers, and (c) Cenozoic metamorphic rims (Figures 8 and 11). Zircon layers are generally interpreted as magmatic when  $\text{Th/U} > 0.3$ , whereas low ratios ( $\text{Th/U} < 0.1$ ) are indicative of metamorphic or near-solidus growth (Teipel et al., 2004; Vavra et al., 1999; Yakymchuk et al., 2018). The porous layers between the core and the outermost rims (Figures 6 and 10) show  $\text{Th/U}$  around 0.1 ( $\pm 0.09$ ). They appear as convoluted zones, black in the CL images, frequently with cavities (see AV19.3 in Figure 6), and sometimes characterized by an “oscillatory damage” (see AN19.6 in Figure 6). We analyzed these layers in migmatitic orthogneisses of the Simano nappe in San Vittore (AV19.3, AV19.4) and in the orthogneisses of the Cima Lunga unit (AG19.5, AN19.6). They usually show Jurassic-Cretaceous ages mostly discordant, hence not considered for U-Pb dating calculations. The high frequency of discordant dates within such porous layers can be due to radioactive damage (metamictization) linked to initial high U-abundance, possibly accompanied by fluid leaching and/or bringing elements into the opened zircon system (Geisler et al., 2007; Harley et al., 2007). These zircon layers indeed show higher U and REE contents (particularly LREE) with respect to the older cores (average of  $^{238}\text{U}$ : 609 ppm for porous layers, 3,884 ppm for inner cores; average of  $\Sigma\text{REE}$ : 1,630 ppm for porous layers, 982 ppm for inner cores; see *Trace\_LAICPMS.xlsx*), and they can contain inclusions.

In addition, these intermediate rims are often damaged by fractures (frequently very thin) which spread into the outer portions of the magmatic Permian cores (Figure 6; AN19.6). These tiny fractures likely served as pathways for selective Pb or U removal, as manifested by the slightly younger dates with respect to the corresponding inner layers of the core. For this reason, in order to get a robust magmatic age for samples AG19.5, AV19.3 and AV19.4, the results from spot analyses positioned in the outer portions of the zircon cores and/or close to cracks were not considered for the calculation of the Concordia age (Figure 7).

The results of SIMS analyses provided age populations comparable to LA-ICP-MS, giving dates that are within-error to 1–2 Ma older (Figure 8). This difference is reduced if a discordia computation approach is applied to SIMS data. The ages computed with “Discordia Model-1” of IsoplotR in the Tera-Wasserburg diagram (see Supporting Information S1 *Tera-Wasserburg\_SIMS.pdf*) are younger than the ones we calculated using our “concordant” approach. The results are 0.2–0.4 Ma younger in sample AV19.3, while 2.5 Ma younger in AV19.4, however with a higher  $2\sigma$  error ( $\pm 3.44$  Ma). This may be due to a higher common Pb present in the latter sample, in which a higher number of discordant data was indeed obtained.

The partial lack of accuracy between methods can be attributed to the difference in the ablated material (SIMS:  $8 \times 10 \mu\text{m}$  vs. LA-ICP-MS: 20–30  $\mu\text{m}$ ). A larger spot may include more unrecognized damaged zones that could have suffered Pb or U loss. Alternatively, the age gap may be explained by the lower number of concordant SIMS analyses. However, the within-error overlap of LA-ICP-MS U-Pb dates at 31 Ma on metamorphic rims over seven samples suggests that a non-systematic effect of zircon damage zones cannot have significantly influenced the final ages and confirms the robustness of our data.

### 5.2. Combining Geological Mapping and Pre-Alpine Zircon U-Pb Ages

#### 5.2.1. The Cima Lunga Unit as a Pre-Variscan Sedimentary Basin

Our geological mapping of the Cima Lunga unit shows a metamorphic unit which apparently still preserves its sedimentary stratigraphy even though it is highly sheared and folded, particularly around the mafic and ultramafic lenses (Maino et al., 2021). In the Cima Lunga unit, we mapped approximately 20 m thick calcschist layers, which are continuous over a distance of 6–10 km (Figures 1, 3, and 4, *Cima di Gagnone*, *Cima di Precastello*). These layers occur together with quartzo-feldspathic layers that we identified as orthogneisses (see results; AG19.5, AN20.1, AN19.6). This continuity of both calcschist and orthogneiss layers contrasts with the spotted arrangement of the mafic and ultramafic rocks, which are more abundant in the upper part of the unit.

The spotted arrangement of mafic and ultramafic rocks was previously interpreted as the result of an Alpine tectonic mélangé and the metasediments of the Cima Lunga unit were interpreted to derive from a Mesozoic Tethyan oceanic basin (Engi et al., 2001; Trommsdorff, 1990; Trommsdorff et al., 2000). However, our U-Pb zircon ages disagree with a Mesozoic origin of the Cima Lunga metasediments since the detrital zircon cores record only pre-Devonian ages and these cores are rimmed by Variscan metamorphic rims (ca. 300–315 Ma, sample *AG20.2*; and 323 Ma, sample *AG19.6*; Figure 6). As already mentioned by Gebauer (1994), the detrital zircon cores from the Cima Lunga paragneisses (*AG19.6*, *AG20.1*, *AG20.2*) have a wide range of ages spanning from Precambrian to Cambro-Ordovician, and the youngest detrital zircon grains are ca. 400 Ma (Figure 10).

A Cambro-Ordovician age for the Cima Lunga basin is also in line with the protolith ages of the dismembered ophiolitic fragments ( $528 \pm 6$  Ma age; zircon U–Pb SHRIMP on a mafic eclogite; Gebauer, 1994). The ages obtained for the ophiolitic fragments are similar to the ages of pre-Variscan ophiolitic rocks that are found within the gneissic basement nappes of both the external massifs and the Central Alps (Schaltegger et al., 2002). Hence, these ophiolitic rocks cannot be correlated with any Tethyan ophiolite.

We infer that also the continuous calcschist layers, which belong to the same pre-Variscan metasedimentary sequence of the Cima Lunga paragneisses, cannot be ascribed to a Mesozoic origin. The calcschist layers occur together with orthogneisses. The protolith ages of orthogneisses at 277–283 Ma (*AG19.5*, *AN20.1*, *AN19.6*, *OS17-013*, *AV19.3*, *AV19.4*) reflect the late Variscan magmatism of the pre-Alpine European basement units. Since these Permian magmatic events are well-documented in both margins of the Alpine Tethys (e.g., Beltrán-Triviño et al., 2013), it is unlikely that a Mesozoic basin within the Penninic domain would not contain any detritism of these Permian events. The pre-Carboniferous ages of a small number of old zircon cores detected in these orthogneisses with Permian protolith would belong to fragments inherited from the surrounding paragneissic country rocks during the intrusion, or to remnants of older molten precursors.

This Permian protolith age answers to a long-standing debate whether the origin of the quartzo-feldspathic gneisses is magmatic or sedimentary (Dal Vesco, 1953; Pfeifer, 1987; Swiss National Map no. 1293 - Osogna (1:25,000)—Note esplicative). Their intra-layer appearance without an evident discordance with the outer paragneissic rocks (e.g., Figure 3) infers that they represented sill-like intrusions in the pre-existing metasedimentary sequence (Figure 12b), being subsequently metamorphosed and sheared with it during the Alpine cycle (Figures 12c–12e). Finally, the continuity over several kilometers of these 10–30 m thick orthogneissic layers (sample *AN20.1*; Figure 3) within calcschists suggests that these layers are not imbricated fragments derived from the Simano nappe.

### 5.2.2. The Cima Lunga Unit Embedded in the Simano Nappe

The transition from the Simano nappe to the Cima Lunga unit up to the Maggia nappe is marked by a non-linear increase in strain (see also Maino et al., 2021). In places, the attribution of the gneissic rocks to either the Simano nappe or the Cima Lunga unit is difficult, suggesting that these lithotypes may belong to the same original tectonostratigraphic sequence. Indeed, as discussed in Section 4, the Permian protoliths of the migmatitic leucogneisses of the Simano nappe (*AV19.3* and *AV19.4*) have magmatic ages contemporaneous within-error to the orthogneissic protolith of the Cima Lunga unit (*AG19.5*, *AN20.1*, *AN19.6*; Figure 7). In addition, in the Simano basement of the San Vittore sequence, the Pre-Alpine garnet-paragneiss (sample *AV19.7*) shows a distribution of ages (older than 500 Ma; see *KDE\_LAICPMS.pdf* in Supporting Information S1) similar to the detritism of the Cima Lunga garnet-paragneisses.

In agreement with these data, in the Cima di Precastello region (Figure 4), the upper part of the Cima Lunga unit is interfingering by locally folded Simano orthogneisses. Below the tectonic contact with the overthrust Maggia nappe (see *profile* in Figure 4), this deformed geometry of interfingering gneisses recalls the intrusion of magmas into paragneisses.

Within a shear zone like the Maggia-Simano tectonic contact, it is difficult to exclude a priori that the Cima Lunga unit may be an independent tectonic slice detached from the Simano nappe or alternatively from the Maggia nappe. However, the actual geometry of the upper Simano nappe and the Cima Lunga unit suggests a coherent inherited large-scale (Permian) magmatic edifice, sheared and folded below the Maggia nappe during nappe emplacement. Similar magmatic relationships can be observed in other parts of the Simano nappe (e.g., the famous Lavertezzo outcrops; Sharma, 1969).

Rütti et al. (2005) suggested that the geometry of the upper Simano nappe may be explained by post-nappe emplacement folding (deformation phase D2) in which the Cima Lunga unit represents the fold core. However, the parasitic folds along the thrust are at odds with this explanation, and at the lower boundary of the Maggia nappe, they depict  $\Omega$ -folds (Figure 4). The  $\Omega$ -folds occurred during extensive partial melting (Sample OS17-013) that likely accommodated part of the deformation during overthrusting. This syn-migmatitic deformation depicts a tectonic boundary that defines the base of the Maggia nappe.

### 5.2.3. The Maggia-Adula Nappe System

Based on our observations, the Maggia nappe rests above the Simano nappe (which includes the Cima Lunga unit) and is on the same tectonostratigraphic level as the Adula nappe further to the east. Both contacts, Maggia-Simano and Adula-Simano, are prominent shear zones that are marked by syn-kinematic migmatitic belts, and where the upper block moved in the same kinematic direction and at the same time (see Sections 5.3 and 5.4).

Along the Adula-Simano nappe contact, a Mesozoic nappe-divider was mapped in the San Vittore region (Figure 5). Inside this sequence, according to the detrital dates, the metaconglomerate AV19.1 is interpreted as a Mesozoic sediment, metamorphosed and deformed within the shear zone. Directly above it, calcschists, marbles and an amphibolite suggest a Triassic sequence of Helvetic affinity in a normal stratigraphic position (Beltrán-Triviño et al., 2013; Gisler et al., 2007), likely belonging to the parautochthonous cover of the Simano nappe. Alternatively, the intense deformation may have put these lithotypes together in Alpine times. This explanation is suggested by the presence of folded lenses of possible Adula origin (*lithologies of unknown age* in Figure 5) in the upper part of the sequence.

Along the Maggia-Simano nappe contact, the shear zone comprises the Cima-Lunga unit (see Section 5.2.2). Further to the west, the Maggia nappe rests above the Antigorio nappe and the Mergoscia zone (Figure 1b). The Mergoscia zone can be considered a shear zone at the base of the Maggia nappe, comparable in metamorphism and in deformation to the Cima Lunga unit (e.g., Steck et al., 2013, 2019). We therefore consider the Maggia-Simano, Adula-Simano, and Maggia-Antigorio contacts to all form part of the same shear zone.

Hence, the architecture of the Lepontine nappes (Figure 12) supports a large-scale Alpine Maggia-Adula nappe that was thrust over the Simano and Antigorio nappes, as already proposed in the early work of Jenny (1923). The geometry of the Maggia-Adula nappe depicts a mirror-like symmetry along the NW-SE central axis of the Ticino culmination (Figure 12a). In the western and northern parts, our reconstruction agrees with the sheath fold model of the Maggia nappe of Steck et al. (2019). However, to the south the Maggia-Adula nappe was disrupted and folded by the migmatites of the SSB and, as a consequence, it appears rootless. Before the intense reworking of the migmatitic belt, the nowadays spatially separated Maggia and Adula nappes presumably formed a laterally continuous Maggia-Adula nappe which was bent in the SSB (Figures 12d and 12e).

The ages of the Permian protolith of the orthogneisses constituting the Maggia and Adula nappes are comparable (Figure 12b). The Cocco and Ruscada orthogneisses in the Maggia nappe mostly show ages at ca. 300–310 Ma (Bussien et al., 2011), and the Zervreila orthogneiss in the Adula nappe at 288–297 Ma (Cavargna-Sani, Epard, Bussy, & Ulianov, 2014). The orthogneisses in the Simano nappe (orthogneisses AV19.3, AV19.4 in this study) show younger ages at 278–282 Ma (Figure 7). Therefore, the similar ages of orthogneisses in the Maggia and Adula sectors of the nappe may also support lateral paleogeographic continuity.

A challenge for the interpretation of a large-scale Maggia-Adula nappe is the absence of HP rocks in its western region, the current Maggia nappe. Schmid et al. (2004) mention that Engi et al. (2001) report eclogitic slices found at the base of the Maggia nappe, but their location is to our knowledge uncertain. Eclogitic mafic rocks are documented only within the Adula nappe, being mostly concentrated on its upper part (see Figures 1b and 12a). However, neither the Adula ortho- nor para-gneisses show evidence of HP mineral assemblages, except for a whiteschist lens (Meyre et al., 1999). Therefore, it cannot be excluded that the orthogneisses of the current Maggia nappe have experienced a similar P-T evolution as the orthogneisses of the current Adula nappe.

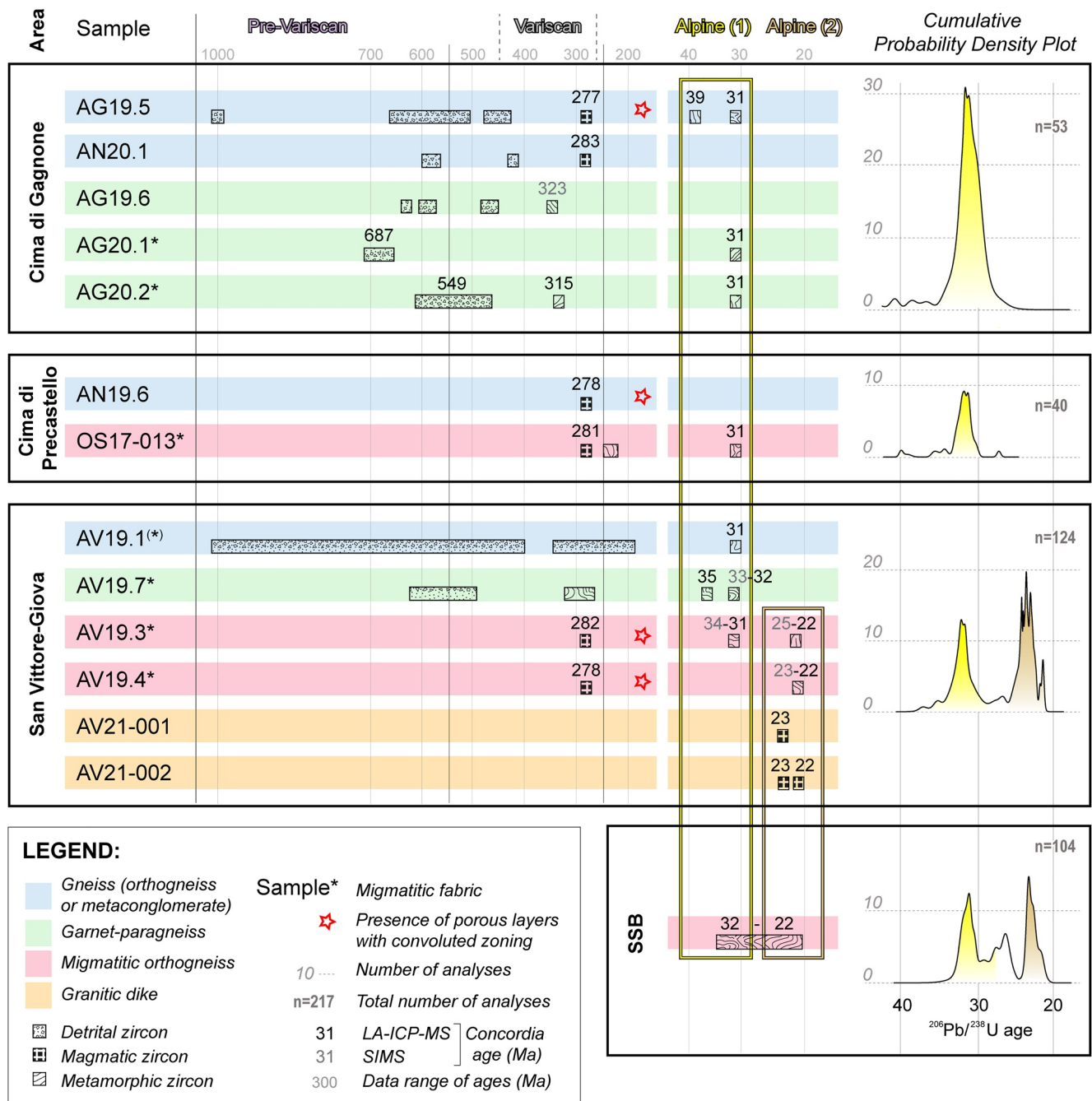


**Figure 10.** Summary of the calculated Concordia ages (both LA-ICP-MS and SIMS ages) and distribution of U-Pb zircon ages. For the distribution of single dates for each sample, see *KDE\_LAICPMS.pdf* in Supporting Information S1.

### 5.3. Combining Geological Mapping and Results on Alpine Zircon Growth

#### 5.3.1. Syn-Tectonic Migmatites on the Sole of the Maggia-Adula Nappe

##### 5.3.1.1. Migmatites Occurrence

The distribution of the syn-tectonic migmatites along the basal shear zone of the Maggia-Adula nappe is not uniform. To the north, in the footwall of the main thrust (*Cima di Gagnone*, Figure 3), Alpine leucosomes occur sporadically in the Cima Lunga paragneisses (samples *AG20.1* and *AG20.2*) and are more localized around the ultramafic lenses (Corvò et al., 2021). Apart from a few domains (see Figure 3), most paragneisses do not show

any migmatitic texture and Alpine zircon rims are absent (e.g., *AG19.6*). Only a few metamorphic zircon rims could be analyzed in the orthogneisses of the Cima Lunga unit (cfr. *AG19.5* with *AN20.1*).

In the central domain (*Cima di Precastello*, Figure 4), widespread metatextitic to diatextitic migmatites were observed in the Maggia orthogneisses at the base of the nappe (*OS17-013*). In the footwall orthogneisses (Simano nappe), only a few migmatites were observed; however, they were not dated. Additionally, the orthogneisses within the base of the Cima Lunga unit (close to the contact with the Simano orthogneisses) do not show any textural evidence for partial melting (*ANI9.6*).

To the south (*San Vittore*, Figure 5), abundant top-to-NW sheared migmatites occur in the orthogneissic footwall and inside the Mesozoic sequence of the Simano nappe. In the hanging wall, the base of the Adula nappe does not show any direct evidence of partial melting, even though foot- and hanging wall rocks have similar compositions (metagranites and paragneisses) and hanging wall rocks experienced hydrous retrogression during deformation.

In summary, the overall picture shows a migmatitic belt with internal variations in the degree of partial melting in coincidence with local lithological heterogeneities. This migmatitic belt occurs along the main basal shear zones of the current Maggia and Adula nappes, which supports our interpretation of a large-scale Maggia-Adula nappe.

#### 5.3.1.2. Migmatization Age

In both orthogneissic and paragneissic migmatites, the REE patterns of zircon rims at ca. 31 Ma show equilibrium with melt. In the migmatitic garnet-paragneisses (samples *AG20.1*, *AG20.2* of Cima di Gagnone and *AV19.7* of San Vittore), thick zircon rims developed mostly in the presence of garnet (Rubatto, 2002; Rubatto & Hermann, 2007), at the beginning of anatectic melt production (absence of Eu anomaly; Figure 9; Hoskin & Schaltegger, 2003; Sawyer, 2008; Trail et al., 2012). In the migmatitic orthogneiss *AV19.3* from San Vittore, zircon rims with high HREE contents and Eu-negative and Ce-positive anomalies (Figure 9) were likely in equilibrium with evolved melts in which plagioclase was already crystallized (Sawyer, 2008) and in the absence of garnet. The absence of garnet in our samples and the extensive migmatization in the orthogneissic migmatites support this geochemical interpretation. In the metaconglomerate *AV19.1* from San Vittore, microtextures typical of incipient partial melting (see *THINSECTIONS\_description.docx* in Supporting Information S1) also suggest zircon crystallization during migmatization.

Hence, the zircon rims at ca. 31 Ma of the Cima Lunga orthogneisses (*AG19.5*) and paragneisses (*AG20.1* and *AG20.2*), of the Simano migmatitic orthogneisses (*AV19.3*) and paragneisses (*AV19.7*), of the Maggia migmatitic orthogneisses (*OS17-013*), and in the metaconglomeratic nappe-divider (*AV19.1*) date the event of partial melting (Figures 8, 10, and 11).

In the Cima di Gagnone region, slightly older ages are reported by Gebauer (1994) on metamorphic zircon domains in kyanite-bearing paragneisses yielding an age of  $33.0 \pm 0.6$  Ma, and by Corvò et al. (2021) on meta-sediments around ultramafic bodies at  $36.0 \pm 1.2$  Ma (Figure 3). Those ages mark local thermal re-equilibration during decompression and local metasomatism of the units (Corvò et al., 2021). A few older rims at ca. 39 Ma age (orthogneissic sample *AG19.5* in the Cima Lunga unit; Figure 8) are within-error contemporaneous to the ca. 40 Ma old HP garnet-lherzolite (Becker, 1993).

In the San Vittore region, the garnet-paragneiss (sample *AV19.7*) also recorded an initial stage of garnet formation, which was followed (and partially coexisted) with the development of the main metamorphic foliation, associated with partial melting. We suggest that these two phases correspond to the growth of zircon rims at ca. 34.7 Ma and ca. 31.5–32.8 Ma, respectively (Figure 8).

#### 5.3.1.3. Post-Migmatization Ages

Another group of ages, younger than the migmatization stage, is recorded only in the San Vittore area (Figure 5). The migmatitic orthogneiss *AV19.3* is the only migmatite sample that registers both ages (Figures 8, 10, and 11). The older zircon crystallization stage, at 31–33.7 Ma, developed in the presence of plagioclase (Figure 9) during the syn-tectonic migmatization event. Younger crystallization ages at 21.9–24.8 Ma are recorded in the metamorphic rims of the most external domains of the zircon. Differently, in sample *AV19.4* (migmatitic orthogneiss), the only recorded (metamorphic) imprint is at 22.5–23.4 Ma (Figures 8, 10, and 11). These rims are characterized by a depletion in REE content (especially MREE), a lower Ce anomaly, and absence of Eu anomaly (Figure 9), confirming that they did not crystallize coeval with plagioclase from a melt, but probably as the result of a metasomatic/hydrothermal process (e.g., Fu et al., 2008; Geisler et al., 2003, 2007; Hoskin, 2005; Hoskin & Black, 2000). The 31 Ma migmatization ages are not recorded in this sample, likely due to a re-equilibration

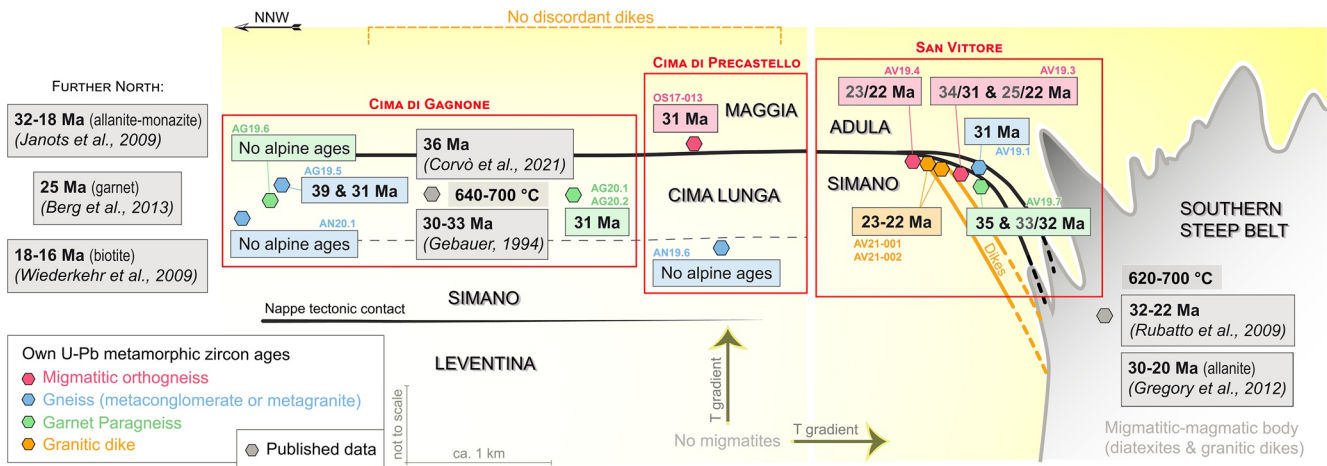


**Figure 11.** Sketched tectonic overview with own data (LA-ICP-MS ages in black/SIMS ages in gray) and some ages from the literature (if not specified, the ages are U-Pb on zircon).  $T$  gradients are qualitatively estimated according to the presence of migmatites in gneissic rocks.

promoted by the close intrusion of two granitic dikes, which could have reset the zircon system in different portions of the rock (Bindeman & Melnik, 2016). The two granitic dikes (samples AV21-001 and AV21-002) were dated at ca. 22–23 Ma (Figures 8, 10, and 11). Their crystallization evolution followed a progressive extreme enrichment in REE (contents  $10^6$  higher than chondritic; Figure 9), and garnet formation (Rubatto, 2002; Rubatto & Hermann, 2007). The geochemistry shows this evolution through time, leading to new zircon growth in the evolving dike (Figures 6 and 9). A similar pegmatite, with zircon grains characterized by extremely low Th/U ratios and intensely altered cores, was dated at  $25.1 \pm 0.6$  Ma north of San Vittore by Gebauer (1996).

### 5.3.2. Timing of the Regional Barrovian Metamorphism: Peak $T$ Conditions at 31 Ma

The whole Lepontine dome is characterized by a highly penetrative NW-SE lineation (Figure 1) with an orientation that corresponds to the top-to-NW shear direction of the syn-tectonic migmatites outcropping along the basal Maggia-Adula shear zone (Figure 5, *San Vittore-Giova*; Figures 2f and 2g). This observation strongly supports the interpretation that lineation and migmatites formed in the same regional strain regime.

In addition, the lineation is defined by the upper amphibolite mineral assemblage and is always at peak metamorphic conditions. The mineral lineation always marks the peak conditions independently of the  $T$  defined by the isograds, which depict concentric shells for the Barrovian metamorphism (Figure 1). The syn-peak constrictional structures are indeed observed both in the Cima di Gagnone area (Figure 3) to the north and in the southernmost studied areas (Figure 4, *Cima di Precastello*; Figure 5, *San Vittore-Giova*), separated by the 650°C isotherm of Todd and Engi (1997) (Figure 1).

Hence, we suggest that lineation, migmatites and isograds developed at the same time at ca. 31 Ma, representing the peak of the regional Barrovian metamorphism in the Lepontine area. In other words, the spatial extent of the regional thermal peak at 31 Ma coincides with the extent of the mineral lineation and can be followed in the field across the Lepontine dome (cfr. Figure 1b with Figure 12a).

In a metamorphic basement like the Lepontine dome, formed by rocks of similar compositions and within a common metamorphic gradient, the front of incipient melting can be considered as an isograd that corresponds to  $T$  of at least 650°C (e.g., Spear, 1993). Temperatures above 650°C at ca. 1 GPa during the local migmatization of the Cima Lunga paragneisses are confirmed by thermo-barometric studies (e.g., Corvò et al., 2021).

One should consider also that fluid inputs along a tectonic contact may slightly lower the melting temperatures. This mechanism has been proposed for the SSB (e.g., Berger et al., 2008), where fluid-induced melting produced the reaction:  $\text{biotite} + \text{plagioclase}_1 + \text{quartz} \pm \text{epidote} + \text{H}_2\text{O} = \text{hornblende} + \text{plagioclase}_2 + \text{melt}_{(\text{feldspar-rich})}$  (Berger et al., 2008). The clear recognizable trace left in the field by this reaction would be the presence of amphiboles in the leucosomes or in the restitic fraction. However, in our field areas, most leucosomes and restites do not bear amphiboles.

Consequently, the melting of migmatites seems not to be due to a fluid-induced mechanism, even though fluids were present in the rocks during deformation. Indeed, above and below the migmatitic belt of the Maggia-Adula shear zone, metagranites and paragneisses contain scattered syn-foliation veins, suggesting the presence of fluids during the formation of the main fabric. The host rocks of these veins do not show signs of migmatization despite the bulk-rock compositions being similar to the protoliths of the migmatites (i.e., the Permian granitic protolith of the orthogneisses, cfr. samples *OS17-013* and *AN19.6* in Figure 4).

The considerations above strongly suggest that migmatization can be taken as a direct  $T$  index and that the border of the migmatitic belt along the Maggia-Adula shear zone can be considered a metamorphic isotherm of at least 650°C.

From our observations (see Section 5.3.1.1), we see that migmatites die out to the north. Consequently, the 650°C isotherm at 31 Ma forms a lobe that wraps the migmatites of the SSB (which have higher temperatures) and closes to the north, where it cuts the tectonic contact (Figure 12d). Considering the shape of the 650°C isotherm, the local paleo-geotherm at 31 Ma depicts an inverted  $T$  gradient across the center of the Lepontine nappe pile. Further north, the lower-grade isotherms (e.g., 600 and 550°C) corresponding to the same temperature field at 31 Ma also plunge into the Simano nappe crosscutting the tectonic contact (Figure 12d).

In the frontal part of the Lepontine dome, prograde allanite U-Th-Pb ages at ca. 32 Ma (Boston et al., 2017; Janots et al., 2009) document an early stage of thrusting at ca. 550°C below the Simano nappe attesting northward migration of the thrusts (Figure 12d). The thrust below the Simano nappe started a new prograde metamorphic cycle up to 620°C registered by Lu-Hf garnet-rutile at 25.4 Ma (Berg et al., 2013) and in the monazite U-Th-Pb ages until ca. 19 Ma (Janots et al., 2009). In some areas of this frontal part, the thermal peak conditions occurred after thrusting (Wiederkehr et al., 2008). We suggest that this  $T$  peak is related to the thermal relaxation of the frontal domain of the nappe stack (Figure 12e).

In the proximity of the SSB (*San Vittore*, Figure 5), new magma intruded at ca. 22–23 Ma. These later intrusion-related ages are recorded in the migmatitic country rock (samples *AV19.3* and *AV19.4*) and in the cross-cutting granitic dikes (samples *AV21-001* and *AV21-002*, Figure 5). In the south, Gebauer (1996) suggests that this magmatic/fluid pulse(s) originated from the SSB within a regional reheating event. However, Rubatto et al. (2009) reported continuous fluid-induced melting from ca. 32 to 22 Ma in the SSB. Hence, during 10 Ma, the SSB was a continuous migmatitic belt from which magmas were escaping into the surrounding regions and formed a belt of discordant dikes (Burri et al., 2005).

Finally, if we consider the whole Lepontine area, monazite U-Pb ages around 22–23 Ma are spread all over the dome (Köppel & Grünenfelder, 1975). These ages are interpreted as the timing of metamorphism close to peak  $T$  conditions at ca. 600°C (Boston et al., 2017) during a second thermal event (Berger et al., 2011). However, in the central domain of the Lepontine dome, these monazite ages cannot record the peak  $T$  condition since U-Pb zircon ages of migmatite record only the 31 Ma event corresponding to peak Barrovian conditions at 650°C or higher. Hence, the young monazite ages may either reflect cooling below ca. 600°C after the peak  $T$  Barrovian event at 31 Ma or a heating event up to ca. 600°C at 22–23 Ma.

The latter case of a heating event does not necessarily need an additional heat source. Indeed, we propose that the top-to-bottom heat diffusion consequent to the inverted thermal gradient at 31 Ma may have slowly heated up the rocks below the Maggia-Adula shear zone until ca. 22–23 Ma.

These cooling or heating scenarios remains disputed and may be tested, for example, by the estimation of cooling rates in garnets using diffusion models. This estimation of cooling rates was recently applied to support the importance of shear heating for two crustal-scale shear zones in Rhodope, Greece and Sikkim, Himalaya (Burg & Moulas, 2022).

## 5.4. Geodynamic Implications

### 5.4.1. Geodynamic Reconstruction

The late Variscan European crust was an old metasedimentary basement intruded in the Permian by magmatic bodies. These magmatic bodies locally formed finger-like intrusions (Figure 12b). A part of this heterogeneous crust was already subducted and exhumed as a sheet-like mélange during the Variscan orogeny (Herwartz

et al., 2011). In our reconstruction, this *mélange* formed the upper region of the crustal units that today corresponds to the Maggia-Adula and Simano nappes. In the Simano nappe, this *mélange* unit forms now mainly the Cima Lunga unit.

In late Variscan time, the Cima Lunga unit could have been part of the same *mélange* region of the Mergoscia zone. The Mergoscia zone represents the upper part of the late Variscan crustal unit that today forms the Antigorio nappe. A lateral correlation between the Mergoscia zone and the Cima Lunga unit (Figures 12a and 12b) is possible but very speculative since the Mergoscia zone is dominated by orthogneisses and the origin of its eclogitic lenses remains unclear.

The geometry of the late Variscan crust was modified during the Mesozoic extension, but we assume that the first-order paleogeographic relations were not significantly changed. During the Alpine convergence, the thinned late Variscan crust, which was part of the European passive margin, was subducted in the Paleogene. Exhumation started around 38 Ma according to the (U)HP event of Herwartz et al. (2011) and Sandmann et al. (2014), when the thrusting of the Maggia-Adula nappe over the Simano nappe began (Figure 12c). The Alpine eclogitic conditions in the Maggia-Adula nappe were reached in the central part of the nappe, whereas in the northernmost regions only pre-Alpine conditions are recorded (Lu-Hf on garnet in Herwartz et al. (2011) and Sandmann et al. (2014)). The exhumation of the Maggia-Adula nappe may have occurred mainly due to buoyancy forces (Candioti et al., 2021; Chemenda et al., 1996; Schmalholz & Schenker, 2016; Vaughan-Hammon et al., 2022), whereby exhumation velocities were likely higher than the horizontal convergence-related velocities (e.g., Dewey et al., 1989; Handy et al., 2015; Schmid et al., 1996).

The shear zone that eventually formed the basal thrust of the Maggia-Adula nappe was initiated in the region of the *mélange* unit that now forms the Cima Lunga unit and the Mergoscia zone (Figures 12b and 12c). Hence, the Cima Lunga unit and the Mergoscia zone were strongly sheared during the overthrusting and exhumation of the Maggia-Adula nappe (Figure 12c). Due to the mechanical heterogeneities as well as the intense and partly strongly localized deformation during overthrusting, the local pressure values likely deviated from the lithostatic pressure estimates (e.g., Moulas et al., 2019; Schmalholz & Podladchikov, 2013). However, the magnitude of such pressure deviations is difficult to constrain and remains disputed (e.g., Pleuger & Podladchikov, 2014; Schenker et al., 2015; Tajčmanová et al., 2021). For example, in the Cima Lunga unit, the differential stresses (Figure 12c) may have locally caused significant tectonic pressures and shear heating around the rheological anomalies of mafic and ultramafic eclogites (Corvò et al., 2021; Maino et al., 2021; Schmalholz et al., 2014). Indeed, HP, HT and chemical variations within the Cima Lunga unit are concentrated around and within the ultramafic and eclogitic bodies. Corvò et al. (2021) show that these variations reflect a heterogeneous metamorphism which is locally developed rather than locally preserved, invoking local tectonic pressures and shear heating.

The overthrusting and exhumation of the Maggia-Adula nappe continued until 31 Ma and generated the syn-thrusting migmatites along the Maggia-Adula basal shear zone and the intense folding of the Cima Lunga unit. The frontal part of the Maggia-Adula nappe reached upper crustal levels at  $31.4 \pm 0.9$  Ma (Rb-Sr geochronology; Ring & Glodny, 2021), where tangential top-to-E normal faults facilitated the uplift of the nappe. At the same time, thrusting of the Simano nappe was active deeper in the crust, at ca. 550°C (Boston et al., 2017; Gieré et al., 2011; Janots et al., 2009). More southward, the upwelling of migmatites along the SSB began a long-lasting melting history (Rubatto et al., 2009). This upwelling is likely responsible for the exhumation of other (U)HP lenses at the Alpe Arami and Monte Duria (Figure 12d; e.g., Hermann et al., 2006). These pulses of uprising melt continued until 22 Ma, when new fluid influxes and melting (Gregory et al., 2012; Rubatto et al., 2009) were accompanied by dike intrusions in the portions of the nappes close to the SSB (Figure 12e; this study; Gebauer, 1996). At this stage, the underplating of more internal units (e.g., Leventina and Gotthard nappes) accompanied the uplift and cooling of the whole nappe edifice, reflected in the U-Th-Pb monazite ages until ca. 19 Ma (Boston et al., 2017). Along the NSB, the peak *T* metamorphism may indeed be related to the underplating of the hot lower units with their sedimentary cover, documented from 25 Ma (Berg et al., 2013) to ca. 20 Ma (e.g., Berger et al., 2011; Janots et al., 2009; Wiederkehr et al., 2008).

#### 5.4.2. Heat Transfer Mechanisms

In our interpretation, a significant amount of heat can be advected due to exhumation and emplacement of the Maggia-Adula nappe (Figure 12). A simple method to estimate the relative importance of advection and diffusion

(conduction) during heat transfer is the application of dimensional analysis and the calculation of dimensionless numbers (e.g., Duprat-Oualid et al., 2015; Turcotte & Schubert, 2014).

For example, the Péclet number quantifies, to first order, the relative contribution of advection and diffusion. The Péclet number is calculated as:  $Pe = (h \cdot v) / D$ , where  $h$  is the thickness of the nappe,  $v$  is the velocity of emplacement and  $D$  is the thermal diffusivity (England & Thompson, 1984; Molnar & England, 1990). Typical values of  $D$  for rocks are approximately  $10^{-6} \text{ m}^2/\text{s}$  (e.g., Turcotte & Schubert, 2014). Based on our field studies, we estimate ca. 7 km for the thickness,  $h$ , of the Maggia-Adula nappe. To estimate  $v$ , we assume that the exhumation of the Maggia-Adula nappe started at ca. 38 Ma (Herwartz et al., 2011; Sandmann et al., 2014; Figure 12c), until ca. 31 Ma (Figure 12d). The Alpine eclogites and ultramafics reached pressures of ca. 1.7–2.2 GPa (Dale & Holland, 2003; Herwartz et al., 2011), which corresponds to ca. 65–80 km depth considering lithostatic pressures and a rock density of  $2,700 \text{ kg}\cdot\text{m}^{-3}$ , and were exhumed to ca. 20 km depth (0.55 GPa; Herwartz et al., 2011). Since deviations from lithostatic pressure are supported by many authors as a possible mechanism acting in a subduction geodynamic scenario (e.g., Pleuger & Podladchikov, 2014; Schenker et al., 2015), we consider a slightly reduced vertical exhumation (ca. 10 km less than the purely lithostatic depth calculation). Assuming a subduction zone with ca. 45-degree dip (Figure 12c), a vertical exhumation of ca. 60 km corresponds to an oblique exhumation along the subduction zone of ca. 85 km. An exhumation along 85 km within 7 Ma provides a velocity of ca. 1.2 cm/a. A faster velocity of ca. 2.8 cm/a is obtained if we assume exhumation within only 3 Ma, as was considered by Piccoli et al. (2021) for the Cima Lunga unit on the basis of U-Pb SHRIMP zircon dating of Hermann et al. (2006) obtained on Monte Duria garnet-peridotite. Velocities of 1.2 and 2.8 cm/a, a thickness of 7 km and a diffusivity of  $10^{-6} \text{ m}^2/\text{s}$  yield values of the Péclet number of 2.7 and 6.2, respectively. Such values of  $Pe$ , somewhere between 1 and 10, show that advection is dominating heat transfer over diffusion, but also that diffusion is still significant to heat the underlying Simano nappe during thrusting. Such syn-tectonic diffusion can generate isograds cross-cutting the nappe boundaries (see results of thermo-kinematic numerical models in Supporting Information S1: *folder TK\_model*). For comparison, values of  $Pe$  for subducting oceanic slabs, where isotherms are nearly parallel to the slab boundaries because of insignificant diffusion, are typically between 100 and 300, mainly due to larger values of  $h$ , representing the thickness of an entire slab, and faster values of  $v$  up to 10 cm/a.

The syn-tectonic partial melting may be supported by a potential localized heat surplus along the main Maggia-Adula basal shear zone and inside the deforming nappes, which could be explained by the heat production related to shear heating (Burg & Gerya, 2005). Many studies suggested that shear heating might produce enough heat to contribute to Barrovian  $T$  between 500 and 700°C (e.g., Burg & Gerya, 2005; Burg & Schmalholz, 2008; Duprat-Oualid et al., 2015; Hartz & Podladchikov, 2008; Maino et al., 2015, 2020; Nabelek et al., 2010; Souche et al., 2013), and shear heating is not negligible along the subduction plate interface (England & Smye, 2022; Smye & England, 2022). However, the contribution of shear heating is still debated (Mako & Caddick, 2018; Platt, 2015; Todd & Engi, 1997). The relative importance of shear heating and diffusion can be estimated with the Brinkman number, which can be calculated as:  $Br = (\eta \cdot v^2) / (k \cdot T)$ , where  $\eta$  is the effective rock viscosity,  $k$  is the thermal conductivity and  $T$  is the representative ambient temperature (Brinkman, 1951; Kiss et al., 2019; Yuen et al., 1978). Values of  $Br$  are more difficult to estimate than values of  $Pe$  because  $Br$  depends on  $\eta$  and its value can vary by several orders of magnitude depending on which flow laws are assumed. Furthermore, values of  $\eta$  can vary significantly within the exhuming and overthrusting nappes due to lithological heterogeneities. For example, recent numerical simulations of Vaughan-Hammon et al. (2022) show variations in  $\eta$  in the exhuming rock units between  $10^{19}$  and  $10^{22}$  Pa·s. Assuming  $k = 2.5 \text{ W/m}\cdot\text{K}$ ,  $T = 873 \text{ K}$  and  $v = 2 \text{ cm/a}$ , then  $\eta = 10^{19}$  Pa·s yields  $Br = 0.002$  and  $\eta = 10^{22}$  Pa·s yields  $Br = 1.8$ . Shear heating should not be completely neglected for heat transfer if  $Br > 0.1$ , which means that  $\eta > 10^{21}$  Pa·s is required for shear heating to be able to contribute to the heat transfer. The applied formulation of  $Br$  assumes a constant velocity. However, magnitudes of  $v$  can have a temporary significant variation, for example, during episodic aseismic (/seismic) slip events. Furthermore, the applied formulation of  $Br$  does not consider the thickness of the deforming zone or the magnitude of the deviatoric stress,  $\tau$ . An alternative formulation is  $Br = (\tau^2 \cdot h^2) / (k \cdot T \cdot \eta)$ , which is also referred to as the Grunfest number (e.g., Kiss et al., 2019), and assumes a constant stress inside a deforming region with a specific thickness. Assuming  $h = 7 \text{ km}$ ,  $k = 2.5 \text{ W/m}\cdot\text{K}$ ,  $T = 873 \text{ K}$ ,  $\tau = 50 \text{ MPa}$  and  $\eta = 10^{20}$  Pa·s, the formulation yields  $Br = 0.56$ . Larger values of  $\eta$  yield smaller values of  $Br$  in this formulation because  $\tau$  is kept constant. Moreover, another formulation for  $Br$  without  $\eta$  is  $Br = (\tau \cdot e \cdot h^2) / (k \cdot T)$  where  $e$  is the shearing rate (e.g., Kiss et al., 2019). Using the same values as before,  $e = 10^{-13} \text{ s}^{-1}$  provides  $Br = 0.11$ . For the assumed values, the magnitude of viscous dissi-

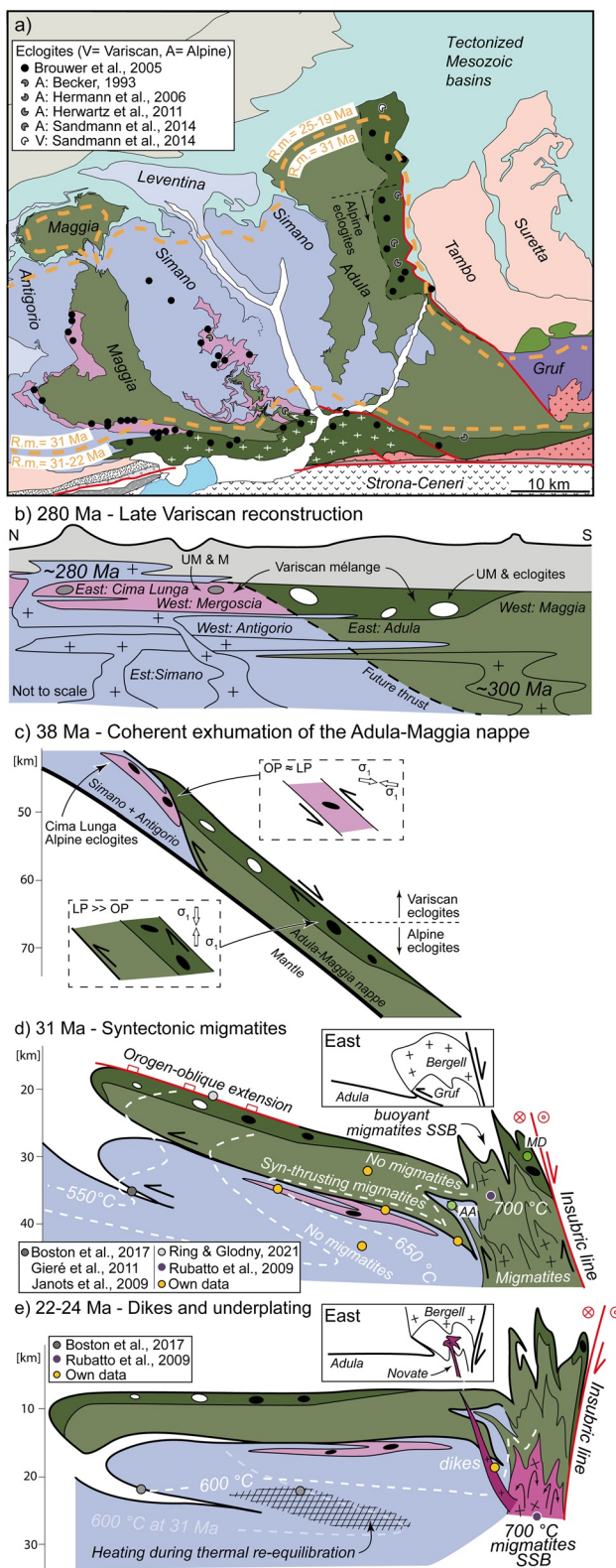


Figure 12.

pation, which is the product of stress times shearing rate,  $\tau \cdot e = 5 \times 10^{-6} \text{ W/m}^3$ . Consequently, if the viscous dissipation inside the nappes during overthrusting is on average larger than approximately  $5 \times 10^{-6} \text{ W/m}^3$ , then shear heating likely impacts heating and the metamorphism. For comparison, the mean value of radiogenic heat production in granites is  $3.7 \times 10^{-6} \text{ W/m}^3$  (e.g., Hasterok & Webb, 2017). Estimating the relative importance of shear heating based on the magnitudes of viscous dissipation likely provides the most robust estimate, because it does not depend on the rock viscosity, which is highly uncertain, as mentioned above, and due to its dependence on mineral composition, fluid content, or grain size. However, due to the many uncertainties and the only first-order estimates from dimensional analysis, more elaborate methods must be applied to quantify the impact of shear heating.

## 6. Conclusions

We applied a combined approach including detailed geological mapping, multi-scale structural analysis, U-Pb zircon dating (LA-ICP-MS and SIMS ion probe analyses) and geochemistry to better constrain the tectono-metamorphic processes responsible for the Barrovian metamorphism of the Lepontine dome. Based on our results, we propose the following conclusions:

1. The regional Barrovian metamorphic event in the Lepontine dome occurred at ca. 31 Ma together with the peak  $T$  conditions manifested by the regional occurrence of migmatites along the major Maggia-Adula shear zone inside the dome, and a penetrative lineation all over the dome. These migmatites indicate a peak  $T$  of at least  $650^\circ\text{C}$ . The younger U-Th-Pb monazite ages until ca. 22 Ma from previous studies throughout the Lepontine dome at lower  $T$  of ca.  $600^\circ\text{C}$  result from the thermal re-equilibration of the nappe pile after the thermal peak at ca. 31 Ma. In contrast, only in the southern part of the dome, along the SSB, published migmatite ages indicate continuous Barrovian high temperatures greater than  $650^\circ\text{C}$  between 31 and 22 Ma. These migmatites injected melt at 22–24 Ma into their close surroundings.
2. The Cima Lunga unit is not an Alpine tectonic mélangé and does not consist of Mesozoic meta-sedimentary rocks. We suggest that the Cima Lunga unit was a pre-Variscan sedimentary sequence that was intruded by Permian magmas, which are the protoliths of the orthogneisses of the Simano nappe. This hypothesis is based on (a) the absence of Variscan and younger zircon detrital ages (<ca. 400 Ma) within the Cima Lunga unit and the Simano nappe (b) the Variscan (ca. 300–320 Ma), metamorphic zircon rims around detrital zircon grains in the Cima Lunga paragneisses, (c) the ca. 280 Ma zircon magmatic ages of continuous orthogneissic horizons (likely intruded as sills) within a calcschist-bearing sequence of the Cima Lunga unit and (d) the protoliths of the ophiolitic fragments within the Cima Lunga unit which are older than Cambrian, as shown by previous studies. Therefore, we suggest that the rocks forming the Cima Lunga unit and the Simano nappe belonged to the same Permian crustal unit.
3. We suggest a single Alpine Maggia-Adula nappe. This correlation is mainly based on (a) the same structural position of the actual Adula and Maggia nappes in the tectonic pile, (b) the same U-Pb metamorphic zircon ages in syn-tectonic migmatites along the basal Maggia-Adula shear zone, (c) the same kinematics, and (d) lithological affinities, such as similar ages of pre-Alpine intrusions. We further correlate the Antigorio nappe with the Simano nappe and the Mergoscia zone with the Cima Lunga unit. The Mergoscia zone and Cima Lunga unit were presumably in the upper regions of the Late Variscan crustal units which form the Antigorio and Simano nappes, respectively. Consequently, we explain the first-order nappe structure of the Lepontine dome with a single exhumation and overthrusting event that ended at ca. 31 Ma. The more deeply

**Figure 12.** Geodynamic evolution of the Lepontine nappes. References for depth- and  $T$ -estimates, and literature ages are mentioned in the main text. (a) Tectonic map of the Lepontine area. The orange dashed lines delimit the areas with common coeval regional metamorphism (R.m). Note that the area delimited by the 31 Ma peak regional metamorphic event coincides with the area of distribution of the constant NW-SE oriented mineral lineation (cfr. with Figure 1b). The Cima Lunga unit and the Mergoscia zone are indicated in violet. The dots indicate eclogites (see legend in the figure). (b) Paleogeographic reconstruction in Permian time of the crust prior to the Alpine cycle. This subplot shows the magmatic relations between Permian granitic bodies and the basement. Mafic (M), ultramafic (UM) and eclogitic bodies are indicated with white and gray ellipses. (c) Beginning of overthrusting during the coherent exhumation of the Maggia-Adula nappe over the Simano and Antigorio nappes. The position of the Cima Lunga unit corresponds to the main shear zone. Shear senses and related local stress fields are indicated in the dashed squares (OP: overpressure, LP: lithostatic pressure). Eclogites are indicated with ellipses: black for Alpine eclogites and white for Variscan eclogites. (d) Internal structure of the Lepontine nappe stack at the regional peak Barrovian conditions at 31 Ma. The white dashed lines represent the indicative isotherms. In the box: a section of the eastern sector, after Galli et al. (2012). AA: Alpe Arami; MD: Monte Duria. (e) Overall thermal re-equilibration of the Lepontine dome. The relaxation of the isotherms (cfr. the white dashed line with the line in transparency) corresponds to local heating. In the box: a section of the eastern sector, the age of Novate granite is after Liati et al. (2000).

subducted Maggia-Adula nappe was thrust over the shallower Simano-Antigorio nappe. During overthrusting, the Mergoscia zone and the Cima Lunga unit were strongly deformed along the basal shear zone of the Maggia-Adula nappe. The subsequent up-arching of the Lepontine dome, the intense deformation along the SSB and erosion caused the present-day geographical separation of the Maggia and Adula nappes.

4. Finally, the heat of the Barrovian metamorphism of the Lepontine dome derives mainly from advection associated with exhumation and thrusting of the Maggia-Adula deeper nappe over the shallower Simano-Antigorio nappe. Heat diffusion during nappe emplacement caused isograds cross-cutting the major nappe boundary between the Maggia-Adula and Simano-Antigorio nappes. Shear heating along this basal shear zone and inside the overthrusting nappe may have contributed to Barrovian heating.

## Data Availability Statement

The supplementary material comprises:

1. detailed description of the methodology adopted in this study (*Methodology.docx*);
2. geological maps of the studied areas with relevant geological sections at the same scale (extended version of Figures 3–5), with stereographic projections of foliation and lineation (*Maps\_extended.pdf*);
3. description of thin sections realized on the samples investigated in this study (*THINSECTIONS\_description.docx*);
4. Excel tables containing the results of analyses for U-Pb dating on zircon crystals with LA-ICP-MS and SIMS probe (*folder UPb\_LAICPMS* and *file UPb\_SIMS.xlsx*);
5. Excel table containing the results of trace element analyses using LA-ICP-MS on zircon crystals (*file Trace\_LAICPMS.xlsx*);
6. Kernel Density Estimates of LA-ICP-MS dates for all samples (*KDE\_LAICPMS.pdf*);
7. Tera-Wasserburg plots for selected SIMS data (*Tera-Wasserburg\_SIMS.pdf*);
8. Excel tables containing the analyses on the standards adopted for LA-ICP-MS analyses (GJ1, Plesovice and SRM612) and relevant Concordia plots (*Stds\_LAICPMS.xlsx*);
9. results of thermo-kinematic numerical models realized using Matlab (*figures* in *folder TK\_model*).

The supplementary material is available at the SUPSI Instory (SUPSI INSTitutional repository) via <http://repository.supsi.ch/13754/> with open access.

## References

- Allaz, J., Maeder, X., Vannay, J. C., & Steck, A. (2005). Formation of aluminosilicate-bearing quartz veins in the Simano nappe (Central Alps): Structural, thermobarometric and oxygen isotope constraints. *Schweizerische Mineralogische Und Petrographische Mitteilungen*, 85(2–3), 191–214. <https://doi.org/10.5169/seals-1660>
- Barrow, G. (1893). On an Intrusion of Muscovite-biotite Gneiss in the South-eastern Highlands of Scotland, and its accompanying Metamorphism. *Quarterly Journal of the Geological Society*, 49(1–4), 330–358. <https://doi.org/10.1144/gsl.jgs.1893.049.01-04.52>
- Barrow, G. (1912). On the geology of Lower Dee-side and the southern Highland Border. *Proceedings of the Geologists' Association*, 23(5), 274–290. [https://doi.org/10.1016/s0016-7878\(12\)80018-6](https://doi.org/10.1016/s0016-7878(12)80018-6)
- Becker, H. (1993). Garnet peridotite and eclogite Sm-Nd mineral ages from the Lepontine dome (Swiss Alps): New evidence for Eocene high-pressure metamorphism in the central Alps. *Geology*, 21(7), 599–602. [https://doi.org/10.1130/0091-7613\(1993\)021<0599:GPAESN>2.3.CO;2](https://doi.org/10.1130/0091-7613(1993)021<0599:GPAESN>2.3.CO;2)
- Beltrán-Triviño, A., Winkler, W., & Von Quadt, A. (2013). Tracing Alpine sediment sources through laser ablation U-Pb dating and Hf-isotopes of detrital zircons. *Sedimentology*, 60(1), 197–224. <https://doi.org/10.1111/sed.12006>
- Berg, C. A., Carlson, W. D., & Connelly, J. N. (2013). Strain rates at high temporal resolution from curved inclusion trails in garnet, Passo del Sole, Central Swiss Alps. *Journal of Metamorphic Geology*, 31(3), 243–262. <https://doi.org/10.1111/jmg.12017>
- Berger, A., Burri, T., Alt-Epping, P., & Engi, M. (2008). Tectonically controlled fluid flow and water-assisted melting in the middle crust: An example from the Central Alps. *Lithos*, 102(3–4), 598–615. <https://doi.org/10.1016/j.lithos.2007.07.027>
- Berger, A., Mercolli, I., & Engi, M. (2005). The central Lepontine Alps: Notes accompanying the tectonic and petrographic map sheet Sopra Ceneri (1:100'000). *Schweizerische Mineralogische Und Petrographische Mitteilungen*, 85(2–3), 109–146.
- Berger, A., Schmid, S. M., Engi, M., Bousquet, R., & Wiederkehr, M. (2011). Mechanisms of mass and heat transport during Barrovian metamorphism: A discussion based on field evidence from the Central Alps (Switzerland/northern Italy). *Tectonics*, 30(1), TC1007. <https://doi.org/10.1029/2009TC002622>
- Bindeman, I. N., & Melnik, O. E. (2016). Zircon survival, rebirth and recycling during crustal melting, magma crystallization, and mixing based on numerical modelling. *Journal of Petrology*, 57(3), 437–460. <https://doi.org/10.1093/petrology/egw013>
- Black, L. P., Kamo, S. L., Allen, C. M., Davis, D. W., Aleinikoff, J. N., Valley, J. W., et al. (2004). Improved  $^{206}\text{Pb}/^{238}\text{U}$  microprobe geochronology by the monitoring of a trace-element-related matrix effect; SHRIMP, ID-TIMS, ELA-ICP-MS and oxygen isotope documentation for a series of zircon standards. *Chemical Geology*, 205(1–2), 115–140. <https://doi.org/10.1016/j.chemgeo.2004.01.003>
- Boekhout, F., Spikings, R., Sempere, T., Chiaradia, M., Ulianov, A., & Schaltegger, U. (2012). Mesozoic arc magmatism along the southern Peruvian margin during Gondwana breakup and dispersal. *Lithos*, 146–147, 48–64. <https://doi.org/10.1016/j.lithos.2012.04.015>

## Acknowledgments

The authors thank Tarryn Cawood and Michel Ballèvre for their very detailed and constructive reviews, and Whitney Behr for the editorial handling. The authors further thank Benita Putlitz and Michelle Foley for the help in the laboratories of UNIL, Maria Giuditta Fellin for the access to ETH Zurich laboratories, Anne-Sophie Bouvier and Daniela Rubatto for the preparation and treatment of raw SIMS analyses, Daphné Giacomazzi for the help during field work, and swisstopo for the opportunity to work on the production of the new Swiss National Map. This work was supported by the Swiss National Science Foundation Grant 182041, SUPSI project no. 12RAFGOSO and no. 12RAICARTOTIGR.

- Boston, K. R., Rubatto, D., Hermann, J., Engi, M., & Amelin, Y. (2017). Geochronology of accessory allanite and monazite in the Barrovian metamorphic sequence of the Central Alps, Switzerland. *Lithos*, 286, 502–518. <https://doi.org/10.1016/j.lithos.2017.06.025>
- Bousquet, R., Goffé, B., Henry, P., Le Pichon, X., & Chopin, C. (1997). Kinematic, thermal and petrological model of the Central Alps: Lepontine metamorphism in the upper crust and eclogitisation of the lower crust. *Tectonophysics*, 273(1–2), 105–127. [https://doi.org/10.1016/S0040-1951\(96\)00290-9](https://doi.org/10.1016/S0040-1951(96)00290-9)
- Bousquet, R., Oberhänsli, R., Goffé, B., Wiederkehr, M., Koller, F., Schmid, S. M., et al. (2008). Metamorphism of metasediments at the scale of an orogen: A key to the Tertiary geodynamic evolution of the Alps. *Geological Society Special Publication*, 298(1), 393–411. <https://doi.org/10.1144/SP298.18>
- Brinkman, H. C. (1951). Heat effects capillary flow. *Applied Scientific Research*, A2(1), 120–124. <https://doi.org/10.1007/bf00411976>
- Brouwer, F. M., Burri, T., Engi, M., & Berger, A. (2005). Eclogite relics in the Central Alps: PT-evolution, Lu-Hf ages and implications for formation of tectonic mélange zones. *Schweizerische Mineralogische Und Petrographische Mitteilungen*, 85(2–3), 147–174.
- Brouwer, F. M., & Engi, M. (2005). Staurolite and other aluminous phases in alpine eclogite from the central Swiss Alps: Analysis of domain evolution. *The Canadian Mineralogist*, 43(1), 105–128. <https://doi.org/10.2113/gscanmin.43.1.105>
- Brouwer, F. M., Van de Zedde, D. M. A., Wortel, M. J. R., & Vissers, R. L. M. (2004). Late-orogenic heating during exhumation: Alpine PT trajectories and thermomechanical models. *Earth and Planetary Science Letters*, 220(1–2), 185–199. [https://doi.org/10.1016/S0012-821X\(04\)00050-0](https://doi.org/10.1016/S0012-821X(04)00050-0)
- Buchmann, H. (1953). Geologie und Petrographie des oberen Maggia-Tales zwischen Fusio und Broglio im NW-Tessin: Inauguraldissertation. *Basler Berichthaus*.
- Burg, J. P., & Gerya, T. V. (2005). The role of viscous heating in Barrovian metamorphism of collisional orogens: Thermomechanical models and application to the Lepontine Dome in the Central Alps. *Journal of Metamorphic Geology*, 23(2), 75–95. <https://doi.org/10.1111/j.1525-1314.2005.00563.x>
- Burg, J. P., & Moulas, E. (2022). Cooling-rate constraints from metapelites across two inverted metamorphic sequences of the Alpine-Himalayan belt: evidence for viscous heating. *Journal of Structural Geology*, 156, 104536. <https://doi.org/10.1016/j.jsg.2022.104536>
- Burg, J. P., & Schmalholz, S. M. (2008). Viscous heating allows thrusting to overcome crustal-scale buckling: Numerical investigation with application to the Himalayan syntaxes. *Earth and Planetary Science Letters*, 274(1–2), 189–203. <https://doi.org/10.1016/j.epsl.2008.07.022>
- Burri, T., Berger, A., & Engi, M. (2005). Tertiary migmatites in the Central Alps: Regional distribution, field relations, conditions of formation and tectonic implications. *Schweizerische Mineralogische Und Petrographische Mitteilungen*, 85(2–3), 215–232.
- Bussien, D., Bussy, F., Magna, T., & Masson, H. (2011). Timing of Palaeozoic magmatism in the Maggia and Sambuco nappes and paleogeographic implications (Central Lepontine Alps). *Swiss Journal of Geosciences*, 104(1), 1–29. <https://doi.org/10.1007/s00015-010-0049-6>
- Candioti, L. G., Duret, T., Moulas, E., & Schmalholz, S. M. (2021). Buoyancy versus shear forces in building orogenic wedges. *Solid Earth*, 12(8), 1749–1775. <https://doi.org/10.5194/se-12-1749-2021>
- Cavargna-Sani, M., Epard, J. L., Bussy, F., & Ulianov, A. (2014). Basement lithostratigraphy of the Adula nappe: Implications for Palaeozoic evolution and Alpine kinematics. *International Journal of Earth Sciences*, 103(1), 61–82. <https://doi.org/10.1007/s00531-013-0941-1>
- Cavargna-Sani, M., Epard, J. L., & Steck, A. (2014). Structure, geometry and kinematics of the northern Adula nappe (Central Alps). *Swiss Journal of Geosciences*, 107(2–3), 135–156. <https://doi.org/10.1007/s00015-014-0175-7>
- Chemenda, A. I., Mattauer, M., & Bokun, A. N. (1996). Continental subduction and a mechanism for exhumation of high-pressure metamorphic rocks: New modelling and field data from Oman. *Earth and Planetary Science Letters*, 143(1–4), 173–182. [https://doi.org/10.1016/0012-821x\(96\)00123-9](https://doi.org/10.1016/0012-821x(96)00123-9)
- Corvò, S., Maino, M., Langone, A., Schenker, F. L., Piazzolo, S., Casini, L., & Seno, S. (2021). Local variations of metamorphic record from compositionally heterogeneous rocks (Cima di Gagnone, Central Alps): Inferences on exhumation processes of (U)HP–HT rocks. *Lithos*, 390–391, 106126. <https://doi.org/10.1016/j.lithos.2021.106126>
- Coward, M., & Dietrich, D. (1989). Alpine tectonics—An overview. *Geological Society, London, Special Publications*, 45(1), 1–29. <https://doi.org/10.1144/gsl.sp.1989.045.01.01>
- Dale, J., & Holland, T. J. B. (2003). Geothermobarometry, P–T paths and metamorphic field gradients of high-pressure rocks from the Adula Nappe, Central Alps. *Journal of Metamorphic Geology*, 21(8), 813–829. <https://doi.org/10.1046/j.1525-1314.2003.00483.x>
- Dal Vesco, E. (1953). *Genesi e metamorfosi delle rocce basiche e ultrabasiche nell'ambiente mesozonale dell'orogene pennidico: Studio geologico-petrografico della Catena Gaggio-Basal (Cantone Ticino)* (Doctoral dissertation). ETH Zurich.
- Debelmas, J., & Lemoine, M. (1970). The western Alps: Palaeogeography and structure. *Earth-Science Reviews*, 6(4), 221–256. [https://doi.org/10.1016/0012-8252\(70\)90079-6](https://doi.org/10.1016/0012-8252(70)90079-6)
- Della Torre, F., Maggini, L., Bonzanigo, L., Hunziker, J. C., & Joss, M. G. (2015). Foglio 1291 Bosco/Gurin. *Atlante Geologico Della Svizzera*, 1:25000.
- Dewey, J. F., Helman, M. L., Knott, S. D., Turco, E., & Hutton, D. H. W. (1989). Kinematics of the western Mediterranean. *Geological Society Special Publication*, 45(45), 265–283. <https://doi.org/10.1144/GSL.SP.1989.045.01.15>
- Dobrzhinetskaya, L., Green, H. W., & Wang, S. (1996). Alpe Arami: A peridotite massif from depths of more than 300 kilometers. *Science*, 271(5257), 1841–1845. <https://doi.org/10.1126/science.271.5257.1841>
- Duprat-Oualid, S., Yamato, P., & Schmalholz, S. M. (2015). A dimensional analysis to quantify the thermal budget around lithospheric-scale shear zones. *Terra Nova*, 27(3), 163–168. <https://doi.org/10.1111/ter.12144>
- Engi, M., Berger, A., & Roselle, G. T. (2001). Role of the tectonic accretion channel in collisional orogeny. *Geology*, 29(12), 1143–1146. [https://doi.org/10.1130/0091-7613\(2001\)029<1143:ROTTAC>2.0.CO;2](https://doi.org/10.1130/0091-7613(2001)029<1143:ROTTAC>2.0.CO;2)
- England, P. C., & Molnar, P. (1993). The interpretation of inverted metamorphic isograds using simple physical calculations. *Tectonics*, 12(1), 145–157. <https://doi.org/10.1029/92tc00850>
- England, P. C., & Smye, A. J. (2022). Metamorphism and deformation on subduction interfaces: 1. Physical framework. *Geochemistry, Geophysics, Geosystems*, 24, e2022GC010644. <https://doi.org/10.1029/2022GC010644>
- England, P. C., & Thompson, A. B. (1984). Pressure–temperature–time paths of regional metamorphism I. Heat transfer during the evolution of regions of thickened continental crust. *Journal of Petrology*, 25(4), 894–928. <https://doi.org/10.1093/petrology/25.4.894>
- Evans, B. W., & Trommsdorff, V. (1978). Petrogenesis of garnet lherzolite, Cima di Gagnone, Lepontine Alps. *Earth and Planetary Science Letters*, 40(3), 333–348. [https://doi.org/10.1016/0012-821x\(78\)90158-9](https://doi.org/10.1016/0012-821x(78)90158-9)
- Evans, B. W., Trommsdorff, V., & Richter, W. (1979). Petrology of an eclogite-metarodinite suite at Cima di Gagnone, Ticino, Switzerland. *American Mineralogist*, 64(1–2), 15–31.
- Frey, M. (1969). *Die Metamorphose des Keupers von Tafeljura bis zum Lukmanier-Gebiet* (Doctoral dissertation).
- Frey, M., Desmons, J., & Neubauer, F. (1999). The new metamorphic map of the Alps. *Schweizerische Mineralogische und Petrographische Mitteilungen*, 79, 1–230.

- Frey, M., & Ferreiro Mählmann, R. (1999). Alpine metamorphism of the Central Alps. *Schweizerische Mineralogische Und Petrographische Mitteilungen*, 79(1), 135–154.
- Froitzheim, N., Schmid, S. M., & Frey, M. (1996). Mesozoic paleogeography and the timing of eclogite-facies metamorphism in the Alps: A working hypothesis. *Eclogae Geologicae Helveticae*, 89(1), 81.
- Fu, B., Page, F. Z., Cavosie, A. J., Fournelle, J., Kita, N. T., Lackey, J. S., et al. (2008). Ti-in-zircon thermometry: Applications and limitations. *Contributions to Mineralogy and Petrology*, 156(2), 197–215. <https://doi.org/10.1007/s00410-008-0281-5>
- Galli, A., Le Bayon, B., Schmidt, M. W., Burg, J. P., Reusser, E., Sergeev, S. A., & Larionov, A. (2012). U-Pb zircon dating of the Gruf Complex: Disclosing the late Variscan granulitic lower crust of Europe stranded in the Central Alps. *Contributions to Mineralogy and Petrology*, 163(2), 353–378. <https://doi.org/10.1007/s00410-011-0676-6>
- Gebauer, D. (1994). A P-T-t path for some high-pressure ultramafic/mafic rock associations and their felsic country-rocks based on SHRIMP-dating of magmatic and metamorphic zircon domains. Example: Central Swiss Alps. In *Abstracts of the 8th International Conference on Geochronology, Cosmochronology and Isotope Geology. ICOG 8, Berkeley, USA, 5. – 11. 6. 1994, U. S. Geological Survey circular 1107, 109, 1994.* & in Extended Abstract Version for 16th General Meeting of IMA, Pisa, Italy, September 4–9, 1994 (Vol. 139–140).
- Gebauer, D. (1996). A P-T-t path for an (ultra?) high-pressure ultramafic/mafic rock-association and its felsic country-rocks based on SHRIMP-dating of magmatic and metamorphic zircon domains. Example: Alpe Arami (Central Swiss Alps). In *Earth Processes Reading the Isotopic Code, Geophysical Monograph* (Vol. 95, pp. 307–329). American Geophysical Union.
- Gebauer, D. (1999). Alpine geochronology of the Central and Western Alps: New constraints for a complex geodynamic evolution. *Schweizerische Mineralogische Und Petrographische Mitteilungen*, 79(1), 191–208.
- Geisler, T., Rashwan, A. A., Rahn, M. K. W., Poller, U., Zwingmann, H., Pidgeon, R. T., et al. (2003). Low-temperature hydrothermal alteration of natural metamict zircons from the Eastern Desert, Egypt. *Mineralogical Magazine*, 67(3), 485–508. <https://doi.org/10.1180/0026461036730112>
- Geisler, T., Schaltegger, U., & Tomaschek, F. (2007). Re-equilibration of zircon in aqueous fluids and melts. *Elements*, 3(1), 43–50. <https://doi.org/10.2113/gselements.3.1.43>
- Gieré, R., Rumble, D., Günther, D., Connolly, J., & Caddick, M. J. (2011). Correlation of growth and breakdown of major and accessory minerals in metapelites from Campolungo, Central Alps. *Journal of Petrology*, 52(12), 2293–2334. <https://doi.org/10.1093/petrology/egr043>
- Gisler, C., Hochuli, P. A., Ramseyer, K., Bläsi, H., & Schlunegger, F. (2007). Sedimentological and palynological constraints on the basal Triassic sequence in Central Switzerland. *Swiss Journal of Geosciences*, 100(2), 263–272. <https://doi.org/10.1007/s00015-007-1225-1>
- Gregory, C., Buick, I. S., Hermann, J., & Rubatto, D. (2009). Mineral-scale trace element and U–Th–Pb age constraints on metamorphism and melting during the Petermann Orogeny (central Australia). *Journal of Petrology*, 50(2), 251–287. <https://doi.org/10.1093/petrology/egn077>
- Gregory, C. J., Rubatto, D., Hermann, J., Berger, A., & Engi, M. (2012). Allanite behaviour during incipient melting in the southern Central Alps. *Geochimica et Cosmochimica Acta*, 84, 433–458. <https://doi.org/10.1016/j.gca.2012.01.020>
- Grond, R., Wahl, F., & Pfiffner, M. (1995). Mehrphasige alpine Deformation und Metamorphose in der nördlichen Cima-Lunga- Einheit, Zentralalpen (Schweiz) = Polyphase Alpine deformation and metamorphism in the northern Cima Lunga unit, Central Alps (Switzerland). *Schweizerische Mineralogische Und Petrographische Mitteilungen*, 75, 371–386.
- Grujic, D., & Mancktelow, N. S. (1996). Structure of the northern Maggia and Lebendun Nappes, Central Alps, Switzerland. *Eclogae Geologicae Helveticae*, 89(1), 461–504.
- Günthert, A. W., Stern, W. B., & Schwander, H. (1996). The polycyclic evolution of the Penninic Maggia nappe, Central Alps: A summary report. *Schweizerische Mineralogische Und Petrographische Mitteilungen*, 76(1), 1–22.
- Handy, M. R., Schmid, M. S., Bousquet, R., Kissling, E., & Bernoulli, D. (2010). Reconciling plate-tectonic reconstructions of Alpine Tethys with the geological-geophysical record of spreading and subduction in the Alps. *Earth-Science Reviews*, 102(3–4), 121–158. <https://doi.org/10.1016/j.earscirev.2010.06.002>
- Handy, M. R., Ustaszewski, K., & Kissling, E. (2015). Reconstructing the Alps–Carpathians–Dinarides as a key to understanding switches in subduction polarity, slab gaps and surface motion. *International Journal of Earth Sciences*, 104(1), 1–26. <https://doi.org/10.1007/s00531-014-1060-3>
- Harley, S. L., Kelly, N. M., & Möller, A. (2007). Zircon behaviour and the thermal histories of mountain chains. *Elements*, 3(1), 25–30. <https://doi.org/10.2113/gselements.3.1.25>
- Hartz, E. H., & Podladchikov, Y. Y. (2008). Toasting the jelly sandwich: The effect of shear heating on lithospheric geotherms and strength. *Geology*, 36(4), 331–334. <https://doi.org/10.1130/G24424A.1>
- Hasterok, D., & Webb, J. (2017). On the radiogenic heat production of igneous rocks. *Geoscience Frontiers*, 8(5), 919–940. <https://doi.org/10.1016/j.gsf.2017.03.006>
- Heinrich, C. A. (1982). Kyanite-eclogite to amphibolite facies evolution of hydrous mafic and pelitic rocks, Adula nappe, Central Alps. *Contributions to Mineralogy and Petrology*, 81(1), 30–38. <https://doi.org/10.1007/BF00371156>
- Heinrich, C. A. (1986). Eclogite facies regional metamorphism of hydrous mafic rocks in the Central Alpine Adula Nappe. *Journal of Petrology*, 27(1), 123–154. <https://doi.org/10.1093/petrology/27.1.123>
- Hermann, J., Rubatto, D., & Trommsdorff, V. (2006). Sub-solidus Oligocene zircon formation in garnet peridotite during fast decompression and fluid infiltration (Duria, Central Alps). *Mineralogy and Petrology*, 88(1), 181–206. <https://doi.org/10.1007/s00710-006-0155-3>
- Herwartz, D., Nagel, T. J., Munker, C., Scherer, E. E., & Froitzheim, N. (2011). Tracing two orogenic cycles in one eclogite sample by Lu-Hf garnet chronometry. *Nature Geoscience*, 4(3), 178–183. <https://doi.org/10.1038/ngeo1060>
- Herwegh, M., Berger, A., Baumberger, R., Wehrens, P., & Kissling, E. (2017). Large-scale crustal-block-extrusion during late alpine collision. *Scientific Reports*, 7(1), 1–10. <https://doi.org/10.1038/s41598-017-00440-0>
- Hoskin, P. W. O. (2005). Trace-element composition of hydrothermal zircon and the alteration of Hadean zircon from the Jack Hills, Australia. *Geochimica et Cosmochimica Acta*, 69(3), 637–648. <https://doi.org/10.1016/j.gca.2004.07.006>
- Hoskin, P. W. O., & Black, L. P. (2000). Metamorphic zircon formation by solid-state recrystallization of protolith igneous zircon. *Journal of Metamorphic Geology*, 18(4), 423–439. <https://doi.org/10.1046/j.1525-1314.2000.00266.x>
- Hoskin, P. W. O., & Schaltegger, U. (2003). The composition of zircon and igneous and metamorphic petrogenesis. In J. Hancher & P. Hoskin (Eds.), *Zircon, Reviews in mineralogy and geochemistry* (Vol. 53, pp. 27–62). <https://doi.org/10.1515/9781501509322-005>
- Huerta, A. D., Royden, L. H., & Hodges, K. V. (1998). The thermal structure of collisional orogens as a response to accretion, erosion, and radiogenic heating. *Journal of Geophysical Research*, 103(7), 15287–15302. <https://doi.org/10.1029/98jb00593>
- Hurford, A. J. (1986). Cooling and uplift patterns in the Lepontine Alps South Central Switzerland and an age of vertical movement on the Insubric fault line. *Contributions to Mineralogy and Petrology*, 92(4), 413–427. <https://doi.org/10.1007/BF00374424>
- Jackson, S. (2008). LAMTRACE data reduction software for LA-ICP-MS. *Laser Ablation ICP-MS in the Earth Sciences: Current Practices and Outstanding Issues* (Vol. 40, pp. 305–307). Mineralogical Association of Canada.

- Jamieson, R. A., Beaumont, C., Fullsack, P., & Lee, B. (1998). Barrovian regional metamorphism: Where's the heat? *Geological Society Special Publication*, 138(1), 23–51. <https://doi.org/10.1144/GSL.SP.1996.138.01.03>
- Janots, E., Engi, M., Berger, A., Allaz, J., Schwarz, J., & Spandler, C. (2008). Prograde metamorphic sequence of REE minerals in pelitic rocks of the Central Alps: Implications for allanite–monazite–xenotime phase relations from 250 to 610°C. *Journal of Metamorphic Geology*, 26(5), 509–526. <https://doi.org/10.1111/j.1525-1314.2008.00774.x>
- Janots, E., Engi, M., Rubatto, D., Berger, A., Gregory, C., & Rahn, M. (2009). Metamorphic rates in collisional orogeny from in situ allanite and monazite dating. *Geology*, 37(1), 11–14. <https://doi.org/10.1130/g25192a.1>
- Jenny, H. (1923). Über Bau und Entstehung der penninischen Decken. *Eclogae Geologicae Helveticae*, 5.
- Kiss, D., Podladchikov, Y. Y., Duretz, T., & Schmalholz, S. M. (2019). Spontaneous generation of ductile shear zones by thermal softening: Localization criterion, 1D to 3D modelling and application to the lithosphere. *Earth and Planetary Science Letters*, 519, 284–296. <https://doi.org/10.1016/j.epsl.2019.05.026>
- Köppel, V., & Grünenfelder, M. (1975). Concordant U–Pb ages of monazite and xenotime from the Central Alps and the timing of high temperature Alpine metamorphism, a preliminary report. *Schweizerische Mineralogische und Petrographische Mitteilungen*, 55, 129–132.
- Köppel, V., Günthert, A., & Grünenfelder, M. (1981). Patterns of U–Pb zircon and monazite ages in polymetamorphic units of the Swiss Central Alps. *Schweizerische Mineralogische Und Petrographische Mitteilungen*, 61, 97–119.
- Liati, A., Gebauer, D., & Fanning, M. (2000). U–Pb SHRIMP dating of zircon from the Novate granite (Bergell, Central Alps): Evidence for Oligocene–Miocene magmatism, Jurassic/Cretaceous continental rifting and opening of the Valais trough. *Schweizerische Mineralogische Und Petrographische Mitteilungen*, 80(3), 305–316.
- Liati, A., Gebauer, D., & Fanning, C. M. (2009). Geochronological evolution of HP metamorphic rocks of the Adula nappe, Central Alps, in pre-Alpine and Alpine subduction cycles. *Journal of the Geological Society*, 166(4), 797–810. <https://doi.org/10.1144/0016-76492008-033>
- Maino, M., Adamuszek, M., Schenker, F. L., Seno, S., & Dabrowski, M. (2021). Sheath fold development around deformable inclusions: Integration of field-analysis (Cima Lunga unit, Central Alps) and 3D numerical models. *Journal of Structural Geology*, 144, 104255. <https://doi.org/10.1016/j.jsg.2020.104255>
- Maino, M., Casini, L., Boschi, C., Di Giulio, A., Setti, M., & Seno, S. (2020). Time-Dependent heat budget of a thrust from geological records and numerical experiments. *Journal of Geophysical Research: Solid Earth*, 125(3), 1–24. <https://doi.org/10.1029/2019JB018940>
- Maino, M., Casini, L., Ceriani, A., Decarli, A., Di Giulio, A., Seno, S., et al. (2015). Dating shallow thrusts with zircon (U–Th)/He thermochronometry—The shear heating connection. *Geology*, 43(6), 495–498. <https://doi.org/10.1130/G36492.1>
- Mako, C. A., & Caddick, M. J. (2018). Quantifying magnitudes of shear heating in metamorphic systems. *Tectonophysics*, 744, 499–517. <https://doi.org/10.1016/j.tecto.2018.07.003>
- Maxelon, M., & Mancktelow, N. S. (2005). Three-dimensional geometry and tectonostratigraphy of the Pennine zone, Central Alps, Switzerland and Northern Italy. *Earth-Science Reviews*, 71(3–4), 171–227. <https://doi.org/10.1016/j.earscirev.2005.01.003>
- Merle, O., Cobbold, P. R., & Schmid, S. M. (1989). Tertiary kinematics in the Lepontine dome. *Geological Society Special Publication*, 45(1), 113–134. <https://doi.org/10.1144/GSL.SP.1989.045.01.06>
- Meyre, C., De Capitani, C., Zack, T., & Frey, M. (1999). Petrology of high-pressure metapelites from the Adula Nappe (Central Alps, Switzerland). *Journal of Petrology*, 40(1), 199–213. <https://doi.org/10.1093/ptro/40.1.199>
- Meyre, C., Marquer, D., Schmid, S. M., & Ciancaleoni, L. (1998). Syn-orogenic extension along the Forcola fault: Correlation of alpine deformations in the Tambo and Adula nappes (eastern Penninic Alps). *Eclogae Geologicae Helveticae*, 91(3), 409–420.
- Miyashiro, A. (2012). *Metamorphism and metamorphic belts*. Springer Science & Business Media.
- Molnar, P., & England, P. (1990). Temperatures, heat flux, and frictional stress near major thrust faults. *Journal of Geophysical Research*, 95(B4), 4833–4856. <https://doi.org/10.1029/JB095IB04p04833>
- Moulas, E., Schmalholz, S. M., Podladchikov, Y., Tajčmanová, L., Kostopoulos, D., & Baumgartner, L. (2019). Relation between mean stress, thermodynamic, and lithostatic pressure. *Journal of Metamorphic Geology*, 37(1), 1–14. <https://doi.org/10.1111/jmg.12446>
- Nabelek, P. I., Whittington, A. G., & Hofmeister, A. M. (2010). Strain heating as a mechanism for partial melting and ultrahigh temperature metamorphism in convergent orogens: Implications of temperature-dependent thermal diffusivity and rheology. *Journal of Geophysical Research*, 115(12), 1–17. <https://doi.org/10.1029/2010JB007727>
- Nagel, T. J. (2008). Tertiary subduction, collision and exhumation recorded in the Adula nappe, central Alps. *Geological Society, London, Special Publications*, 298(1), 365–392. <https://doi.org/10.1144/sp298.17>
- Nagel, T. J., De Capitani, C., & Frey, M. (2002). Isograds and P–T evolution in the eastern Lepontine Alps (Graubünden, Switzerland). *Journal of Metamorphic Geology*, 20(3), 309–324. <https://doi.org/10.1046/j.1525-1314.2002.00368.x>
- Nimis, P., & Trommsdorff, V. (2001). Revised thermobarometry of Alpe Arami and other garnet peridotites from the Central Alps. *Journal of Petrology*, 42(1), 103–115. <https://doi.org/10.1093/ptrology/42.1.103>
- Oxburgh, E. R., & Turcotte, D. L. (1974). Thermal gradients and regional metamorphism in overthrust terrains with special reference to the eastern Alps. *Schweizerische Mineralogische Und Petrographische Mitteilungen*, 54, 641–662.
- Paquin, J., & Altherr, R. (2001). New constraints on the P–T evolution of the Alpe Arami garnet peridotite body (Central Alps, Switzerland). *Journal of Petrology*, 42(6), 1137–1140. <https://doi.org/10.1093/ptrology/42.6.1119>
- Passchier, C. W., & Trouw, R. A. J. (2005). *Microtectonics* (2nd ed., p. 366). Springer.
- Paterson, S. R., Vernon, R. H., & Tobisch, O. T. (1989). A review of criteria for the identification of magmatic and tectonic foliations in granulites. *Journal of Structural Geology*, 11(3), 349–363. [https://doi.org/10.1016/0191-8141\(89\)90074-6](https://doi.org/10.1016/0191-8141(89)90074-6)
- Pfeifer, H.-R. (1981). A model for fluids in metamorphosed ultramafic rocks III. Mass transfer under amphibolite facies conditions in olivine-enstatite rocks of the Central Alps, Switzerland. *Bulletin de Mineralogie*, 104(6), 834–847. <https://doi.org/10.3406/bulmi.1981.7533>
- Pfeifer, H.-R. (1987). A model for fluids in metamorphosed ultramafic rocks: IV. Metasomatic veins in metaharzburgites of Cima di Gagnone, Valle Verzasca, Switzerland. In *Chemical transport in metasomatic processes* (pp. 591–632). Springer.
- Pfiffner, M., & Trommsdorff, V. (1997). Evidence for high-pressure metamorphosed ophiocarbonate rocks, Cima di Gagnone, Central Alps. *Terra Nova Abstract Supplement*, 1, 26.
- Pfiffner, M., & Trommsdorff, V. (1998). The high-pressure ultramafic-mafic-carbonate suite of Cima Lunga-Adula, Central Alps: Excursions to Cima di Gagnone and Alpe Arami. *Schweizerische Mineralogische Und Petrographische Mitteilungen*, 78(2), 337–354.
- Pfiffner, M. A. (1999). Genese der Hochdruckmetamorphosen ozeanischen Abfolge des Cima Lunga-Einheit (Zentralalpen). In *Diss. ETH* (Vol. 13011). ETHZ.
- Piccoli, F., Lanari, P., Hermann, J., & Pettker, T. (2021). Deep subduction, melting, and fast cooling of metapelites from the Cima Lunga Unit, Central Alps. *Journal of Metamorphic Geology*, 40(1), 121–143. <https://doi.org/10.1111/jmg.12621>
- Platt, J. P. (2015). Influence of shear heating on microstructurally defined plate boundary shear zones. *Journal of Structural Geology*, 79, 80–89. <https://doi.org/10.1016/j.jsg.2015.07.009>

- Pleuger, J., & Podladchikov, Y. Y. (2014). A purely structural restoration of the NFP20-East cross section and potential tectonic overpressure in the Adula nappe (central Alps). *Tectonics*, 33(5), 656–685. <https://doi.org/10.1002/2013TC003409>
- Preiswerk, H. (1918). Geologische Beschreibung der Lepontinischen Alpen, zweiter Teil: Oberes Tessin-und Maggiagebiet. *Beiträge Zur Geologischen Karte Der Schweiz*, 26.
- Ring, U., & Glodny, J. (2021). The importance of tangential motion in the Central Alps: Kinematic analysis and Rb/Sr dating of mylonitic rocks from the Pennine nappes in the eastern Central Alps. *Earth-Science Reviews*, 218, 103644. <https://doi.org/10.1016/j.earscirev.2021.103644>
- Rosenbaum, G., & Lister, G. S. (2005). The Western Alps from the Jurassic to Oligocene: Spatio-temporal constraints and evolutionary reconstructions. *Earth-Science Reviews*, 69(3–4), 281–306. <https://doi.org/10.1016/j.earscirev.2004.10.001>
- Rosenberg, C. L., Bellahsen, N., Rabaute, A., & Girault, J. B. (2021). Distribution, style, amount of collisional shortening, and their link to Barrovian metamorphism in the European Alps. *Earth-Science Reviews*, 222, 103774. <https://doi.org/10.1016/j.earscirev.2021.103774>
- Rubatto, D. (2002). Zircon trace element geochemistry: Partitioning with garnet and the link between U–Pb ages and metamorphism. *Chemical Geology*, 184(1–2), 123–138. [https://doi.org/10.1016/S0009-2541\(01\)00355-2](https://doi.org/10.1016/S0009-2541(01)00355-2)
- Rubatto, D., & Hermann, J. (2007). Experimental zircon/melt and zircon/garnet trace element partitioning and implications for the geochronology of crustal rocks. *Chemical Geology*, 241(1–2), 38–61. <https://doi.org/10.1016/j.chemgeo.2007.01.027>
- Rubatto, D., Hermann, J., Berger, A., & Engi, M. (2009). Protracted fluid-induced melting during Barrovian metamorphism in the Central Alps. *Contributions to Mineralogy and Petrology*, 158(6), 703–722. <https://doi.org/10.1007/s00410-009-0406-5>
- Rütti, R. (2001). Tectono-metamorphic evolution of the Simano-Adula nappe boundary, Central Alps, Switzerland. *Schweizerische Mineralogische Und Petrographische Mitteilungen*, 81(1), 115–129.
- Rütti, R., Marquer, D., & Thompson, A. B. (2008). Tertiary tectono-metamorphic evolution of the European margin during alpine collision: Example of the Leventina Nappe (Central Alps, Switzerland). *Swiss Journal of Geosciences*, 101(Suppl. 1), 157–171. <https://doi.org/10.1007/s00015-008-1278-9>
- Rütti, R., Maxelon, M., & Mancktelow, N. S. (2005). Structure and kinematics of the northern Simano Nappe, Central Alps, Switzerland. *Eclogae Geologicae Helveticae*, 98(1), 63–81. <https://doi.org/10.1007/s00015-005-1148-7>
- Sandmann, S., Nagel, T. J., Herwardt, D., Fonseca, R. O. C., Kurzawski, R. M., Munker, C., & Froitzheim, N. (2014). Lu–Hf garnet systematics of a polymetamorphic basement unit: New evidence for coherent exhumation of the Adula Nappe (Central Alps) from eclogite-facies conditions. *Contributions to Mineralogy and Petrology*, 168(5), 1–21. <https://doi.org/10.1007/s00410-014-1075-6>
- Sawyer, E. W. (2008). *Atlas of migmatites* (Vol. 9, p. 371). The Canadian Mineralogist Special Publication, NRC Research Press.
- Scambelluri, M., Pettko, T., Rampone, E., Godard, M., & Reusser, E. (2014). Petrology and trace element budgets of high-pressure peridotites indicate subduction dehydration of serpentinized mantle (Cima di Gagnone, Central Alps, Switzerland). *Journal of Petrology*, 55(3), 459–498. <https://doi.org/10.1093/petrology/egt068>
- Schaltegger, U., Gebauer, D., & Von Quadt, A. (2002). The mafic-ultramafic rock association of Loderio-Biasca (lower Pennine nappes, Ticino, Switzerland): Cambrian oceanic magmatism and its bearing on early Paleozoic paleogeography. *Chemical Geology*, 186(3–4), 265–279. [https://doi.org/10.1016/S0009-2541\(02\)00005-0](https://doi.org/10.1016/S0009-2541(02)00005-0)
- Schenker, F. L., Schmalholz, S. M., Moulas, E., Pleuger, J., Baumgartner, L. P., Podladchikov, Y. Y., et al. (2015). Current challenges for explaining (ultra)high-pressure tectonism in the Pennine domain of the Central and Western Alps. *Journal of Metamorphic Geology*, 33(8), 869–886. <https://doi.org/10.1111/jmg.12143>
- Schlunegger, F., & Kissling, E. (2015). Slab rollback orogeny in the Alps and evolution of the Swiss Molasse basin. *Nature Communications*, 6(1), 8605. <https://doi.org/10.1038/ncomms9605>
- Schmalholz, S. M., Duretz, T., Schenker, F. L., & Podladchikov, Y. Y. (2014). Kinematics and dynamics of tectonic nappes: 2-D numerical modelling and implications for high and ultra-high pressure tectonism in the Western Alps. *Tectonophysics*, 631(C), 160–175. <https://doi.org/10.1016/j.tecto.2014.05.018>
- Schmalholz, S. M., & Podladchikov, Y. Y. (2013). Tectonic overpressure in weak crustal-scale shear zones and implications for the exhumation of high-pressure rocks. *Geophysical Research Letters*, 40(10), 1984–1988. <https://doi.org/10.1002/grl.50417>
- Schmalholz, S. M., & Schenker, F. L. (2016). Exhumation of the Dora Maira ultrahigh-pressure unit by buoyant uprise within a low-viscosity mantle oblique-slip shear zone. *Terra Nova*, 28(5), 348–355. <https://doi.org/10.1111/ter.12227>
- Schmid, S. M., Fügenschuh, B., Kissling, E., & Schuster, R. (2004). Tectonic map and overall architecture of the Alpine orogen. *Eclogae Geologicae Helveticae*, 97(1), 93–117. <https://doi.org/10.1007/s00015-004-1113-x>
- Schmid, S. M., Pfiffner, O. A., Froitzheim, N., Schönborn, G., & Kissling, E. (1996). Geophysical-geological transect and tectonic evolution of the Swiss-Italian Alps. *Tectonics*, 15(5), 1036–1064. <https://doi.org/10.1029/96tc00433>
- Schmid, S. M., Rück, P., & Schreurs, G. (1990). The significance of the Schams nappes for the reconstruction of the paleotectonic and orogenic evolution of the Penninic zone along the NFP-20 East traverse (Grisons, eastern Switzerland). *Mémoires de la Société géologique de France (1833)*, 156, 263–287.
- Sharma, R. S. (1969). On banded gneisses and migmatites from Lavertezzo and Rozzera (Val Verzasca, Ticino). *Schweizerische Mineralogische Und Petrographische Mitteilungen*, 49, 199–276.
- Sláma, J., Košler, J., Condon, D. J., Crowley, J. L., Gerdes, A., Hanchar, J. M., et al. (2008). Plešovice zircon—A new natural reference material for U–Pb and Hf isotopic microanalysis. *Chemical Geology*, 249(1–2), 1–35. <https://doi.org/10.1016/j.chemgeo.2007.11.005>
- Smye, A. J., & England, P. C. (2022). Metamorphism and deformation on subduction interfaces: 2. Petrological and tectonic implications. *Geochemistry, Geophysics, Geosystems*, 24(1), e2022GC010645. <https://doi.org/10.1029/2022GC010645>
- Souche, A., Medvedev, S., Andersen, T. B., & Dabrowski, M. (2013). Shear heating in extensional detachments: Implications for the thermal history of the Devonian basins of W Norway. *Tectonophysics*, 608, 1073–1085. <https://doi.org/10.1016/j.tecto.2013.07.005>
- Spear, F. S. (1993). *Metamorphic phase equilibria and pressure-temperature-time paths* (pp. 352–356). Mineralogical Society of America Monograph.
- Stampfli, G. M., Mosar, J., Marquer, D., Marchant, R., Baudin, T., & Borel, G. (1998). Subduction and obduction processes in the Swiss Alps. *Tectonophysics*, 296(1–2), 159–204. [https://doi.org/10.1016/S0040-1951\(98\)00142-5](https://doi.org/10.1016/S0040-1951(98)00142-5)
- Steck, A. (1998). The Maggia cross-fold: An enigmatic structure of the lower Penninic nappes of the Lepontine Alps. *Eclogae Geologicae Helveticae*, 91, 333–343.
- Steck, A., Della Torre, F., Keller, F., Pfeifer, H. R., Hunziker, J., & Masson, H. (2013). Tectonics of the Lepontine Alps: Ductile thrusting and folding in the deepest tectonic levels of the Central Alps. *Swiss Journal of Geosciences*, 106(3), 427–450. <https://doi.org/10.1007/s00015-013-0135-7>
- Steck, A., Epard, J. L., & Masson, H. (2019). The Maggia nappe: An extruding sheath fold basement nappe in the Lepontine gneiss dome of the Central Alps. *International Journal of Earth Sciences*, 108(8), 2429–2442. <https://doi.org/10.1007/s00531-019-01771-1>

- Steck, A., & Hunziker, J. (1994). The Tertiary structural and thermal evolution of the Central Alps—Compressional and extensional structures in an orogenic belt. *Tectonophysics*, 238(1–4), 229–254. [https://doi.org/10.1016/0040-1951\(94\)90058-2](https://doi.org/10.1016/0040-1951(94)90058-2)
- Steiner, H. (1984). Radiometrische alterbestimmungen an gesteinen der Maggia-decke (Penninikum der Zentralalpen). *Schweizerische Mineralogische Und Petrographische Mitteilungen*, 64(1–2), 227–259.
- Stipp, M., Stünitz, H., Heilbronner, R., & Schmid, S. M. (2002). The eastern Tonale fault zone: A “natural laboratory” for crystal plastic deformation of quartz over a temperature range from 250 to 700°C. *Journal of Structural Geology*, 24(12), 1861–1884. [https://doi.org/10.1016/S0191-8141\(02\)00035-4](https://doi.org/10.1016/S0191-8141(02)00035-4)
- Swiss National Map n°1273 – Biasca (1:25,000). *Swisstopo*.
- Swiss National Map n°1293 – Osogna (1:25,000). *Swisstopo*.
- Swiss National Map n°1294 Grono (1:25,000). *Swisstopo*.
- Tajčmanová, L., Manzotti, P., & Alvaro, M. (2021). Under pressure: High-pressure metamorphism in the Alps. *Elements*, 17(1), 17–22. <https://doi.org/10.2138/GSELEMENTS.17.1.17>
- Teipel, U., Eichhorn, R., Loth, G., Rohrmüller, J., Höll, R., & Kennedy, A. (2004). U-Pb SHRIMP and Nd isotopic data from the western Bohemian massif (Bayerischer Wald, Germany): Implications for upper Vendian and lower Ordovician magmatism. *International Journal of Earth Sciences*, 93(5), 782–801. <https://doi.org/10.1007/s00531-004-0419-2>
- Thigpen, J. R., Ashley, K. T., & Law, R. D. (2017). Evaluating kinematic displacement rate effects on transient thermal processes in thrust belts using coupled thermomechanical finite-element models. *Geological Society of America, Memoirs*, 213, 1–23.
- Thigpen, J. R., Ashley, K. T., Mako, C., Law, R. D., & Spencer, B. (2021). Interplay between crustal-scale thrusting, high metamorphic heating rates, and the development of inverted thermal-metamorphic gradients: Numerical models and examples from the caledonides of Northern Scotland. *Tectonics*, 40(11), 1–24. <https://doi.org/10.1029/2021TC006716>
- Thompson, A. B., & Ridley, J. R. (1987). Pressure—temperature—time (P—T—t) histories of orogenic belts. *Philosophical Transactions of the Royal Society of London - Series A: Mathematical and Physical Sciences*, 321(1557), 27–45.
- Tilley, C. E. (1925). A preliminary survey of metamorphic zones in the southern Highlands of Scotland. *Quarterly Journal of the Geological Society*, 81(1–4), 100–112. <https://doi.org/10.1144/gsl.jgs.1925.081.01-04.05>
- Todd, C. S., & Engi, M. (1997). Metamorphic field gradients in the Central Alps. *Journal of Metamorphic Geology*, 15(4), 513–530. <https://doi.org/10.1111/j.1525-1314.1997.00038.x>
- Trail, D., Watson, E. B., & Tailby, N. D. (2012). Ce and Eu anomalies in zircon as proxies for the oxidation state of magmas. *Geochimica et Cosmochimica Acta*, 97, 70–87. <https://doi.org/10.1016/j.gca.2012.08.032>
- Trommsdorff, V. (1974). Alpine metamorphism of peridotitic rocks. *Schweizerische Mineralogische Und Petrographische Mitteilungen*, 54, 333–352.
- Trommsdorff, V. (1990). Metamorphism and tectonics in the Central Alps: The Alpine lithospheric mélange of Cima Lunga and Adula. *Memorie della Società Geologica Italiana*, 45, 39–49.
- Trommsdorff, V., Hermann, J., Müntener, O., Pfiffner, M., & Risold, A. C. (2000). Geodynamic cycles of subcontinental lithosphere in the Central Alps and the Arami enigma. *Journal of Geodynamics*, 30(1–2), 77–92. [https://doi.org/10.1016/S0264-3707\(99\)00028-9](https://doi.org/10.1016/S0264-3707(99)00028-9)
- Trümpy, R. (1973). The timing of orogenic events in the Central Alps. *Gravity and tectonics*, 287, 301.
- Tumiati, S., Zanchetta, S., Pellegrino, L., Ferrario, C., Casartelli, S., & Malaspina, N. (2018). Granulite-facies overprint in garnet peridotites and kyanite eclogites of Monte Duria (Central Alps, Italy): Clues from srrilankite- and sapphirine-bearing symplectites. *Journal of Petrology*, 59(1), 115–152. <https://doi.org/10.1093/ptrology/egy021>
- Turcotte, D. L., & Schubert, G. (2014). *Geodynamics* (3rd ed.). Cambridge University Press.
- Ulianov, A., Müntener, O., Schaltegger, U., & Bussy, F. (2012). The data treatment dependent variability of U-Pb zircon ages obtained using mono-collector, sector field, laser ablation ICP-MS. *Journal of Analytical and Atomic Spectrometry*, 27(4), 663–676. <https://doi.org/10.1039/c2ja10358c>
- Vance, J. A. (1961). Polysynthetic twinning in plagioclase. *American Mineralogist*, 46(9–10), 1097–1119.
- Vaughan-Hammon, J. D., Candiotti, L. G., Duret, T., & Schmalholz, S. M. (2022). Metamorphic facies distribution in the Western Alps predicted by petrological–thermomechanical models of syn-convergent exhumation. *Geochemistry, Geophysics, Geosystems*, 23(8), e2021GC009898. <https://doi.org/10.1029/2021GC009898>
- Vavra, G., Schmid, R., & Gebauer, D. (1999). Internal morphology, habit and U-Th-Pb microanalysis of amphibolite-to-granulite facies zircons: Geochronology of the Ivrea Zone (Southern Alps). *Contributions to Mineralogy and Petrology*, 134(4), 380–404. <https://doi.org/10.1007/s004100050492>
- Vermeesch, P. (2018). IsoplotR: A free and open toolbox for geochronology. *Geoscience Frontiers*, 9(5), 1479–1493. <https://doi.org/10.1016/j.gsf.2018.04.001>
- Wenk, E. (1955). Eine Strukturkarte der Tessiner Alpen. *Schweizerische Mineralogische Und Petrographische Mitteilungen*, 35, 311–319.
- Wenk, E., & Keller, F. (1969). Isograde in Amphibolitserien der Zentralalpen. *Schweizerische Mineralogische Und Petrographische Mitteilungen*, 49, 157–198.
- Wiederkehr, M., Bousquet, R., Schmid, S. M., & Berger, A. (2008). From subduction to collision: Thermal overprint of HP/LT meta-sediments in the north-eastern Lepontine Dome (Swiss Alps) and consequences regarding the tectono-metamorphic evolution of the Alpine orogenic wedge. *Swiss Journal of Geosciences*, 101(Suppl. 1), 127–155. <https://doi.org/10.1007/s00015-008-1289-6>
- Wiederkehr, M., Bousquet, R., Ziemann, M. A., Berger, A., & Schmid, S. M. (2011). 3-D assessment of peak-metamorphic conditions by Raman spectroscopy of carbonaceous material: An example from the margin of the Lepontine dome (Swiss Central Alps). *International Journal of Earth Sciences*, 100(5), 1029–1063. <https://doi.org/10.1007/s00531-010-0622-2>
- Wiederkehr, M., Sudo, M., Bousquet, R., Berger, A., & Schmid, S. M. (2009). Alpine orogenic evolution from subduction to collisional thermal overprint: The <sup>40</sup>Ar/<sup>39</sup>Ar age constraints from the Valaisan Ocean, central Alps. *Tectonics*, 28(6), TC6009. <https://doi.org/10.1029/2009TC002496>
- Winter, J. D. (2013). *Principles of igneous and metamorphic petrology*. Pearson Education.
- Yakymchuk, C., Kirkland, C. L., & Clark, C. (2018). Th/U ratios in metamorphic zircon. *Journal of Metamorphic Geology*, 36(6), 715–737. <https://doi.org/10.1111/jmg.12307>
- Yuen, D. A., Fleitout, L., Schubert, G., & Froidevaux, C. (1978). Shear deformation zones along major transform faults and subducting slabs. *Geophysical Journal of the Royal Astronomical Society*, 54(1), 93–119. <https://doi.org/10.1111/j.1365-246X.1978.tb06758.x>
- Zanchetta, S., Garzanti, E., Doglioni, C., & Zanchi, A. (2012). The Alps in the Cretaceous: A doubly vergent pre-collisional orogen. *Terra Nova*, 24(5), 351–356. <https://doi.org/10.1111/j.1365-3121.2012.01071.x>

### References From the Supporting Information

- Jochum, K. P., Weis, U., Stoll, B., Kuzmin, D., Yang, Q., Raczek, I., et al. (2011). Determination of reference values for NIST SRM 610-617 glasses following ISO guidelines. *Geostandards and Geoanalytical Research*, 35(4), 397–429. <https://doi.org/10.1111/j.1751-908X.2011.00120.x>
- Klein, C., Hurlbut, C. S., Dana, J. D., & Mineralog, G. (1993). *Manual of mineralogy* (Vol. 394). Wiley.
- Li, X., Long, W., Li, Q., Liu, Y., Zheng, Y., Yang, Y., et al. (2010). Penglai zircon megacrysts: A potential new working reference material for microbeam determination of Hf–O isotopes and U–Pb age. *Geostandards and Geoanalytical Research*, 34(2), 117–134. <https://doi.org/10.1111/j.1751-908X.2010.00036.x>
- McDonough, W. F., & Sun, S. s. (1995). The composition of the Earth. *Chemical Geology*, 120(3–4), 223–253. [https://doi.org/10.1016/0009-2541\(94\)00140-4](https://doi.org/10.1016/0009-2541(94)00140-4)